Progress in Oceanography 235 (2025) 103481

Contents lists available at ScienceDirect

Progress in Oceanography

journal homepage: www.elsevier.com/locate/pocean

Connection of central South China Sea current variability with tropical Rossby waves in the western North Pacific

Mac Euan D. Malugao [a,b,d], Sen Jan [a,b,*], Ming-Huei Chang [b], Tung-Yuan Ho [a,b,c], Yiing Jang Yang [b]

[a] Taiwan International Graduate Program (TIGP)-Earth System Science Program, Academia Sinica and National Taiwan University, Academia Sinica, Taipei 115201, Taiwan, ROC
[b] Institute of Oceanography, National Taiwan University, Taipei 106319, Taiwan, ROC
[c] Research Center for Environmental Changes, Academia Sinica, Taipei 115201, Taiwan, ROC
[d] Department of Marine Science, College of Science and Mathematics, Mindanao State University-Iligan Institute of Technology, Iligan City 9200, Philippines

ARTICLE INFO

Keywords:
South China Sea
Philippine Archipelago
Rossby waves
Intraseasonal oscillation
Sea level anomaly
Transmission

ABSTRACT

This study investigates the connection between the current velocity variations in the central South China Sea (SCS) and westward-propagating tropical Rossby waves in the western North Pacific, using satellite altimeter observations and coastal tide-gauge data supplemented by numerical modeling. This work is focused on the dynamic link between the intraseasonal velocity oscillations observed in the central-eastern SCS in summer 2017 and the Rossby waves that impinge on the east coast of the Philippine Archipelago. Low-pass-filtered satellite sea level anomaly (SLA) data and coastal sea level records suggest that Rossby waves can propagate into the Celebes Sea and Sulu Sea, eventually reaching the central SCS. A three-dimensional, primitive equation model shows that Rossby wave-associated SLA signals transmit through the Philippine Archipelago to the central SCS via the Celebes Sea-Sibutu Passage-Sulu Sea-Mindoro Strait route, with modeled SLA propagation timings that are consistent with the observations. As the Rossby wave reaches the eastern Philippines, approximately one-third of the incident wave energy from a meridional section east of the Philippines (132°E, between 2°N and 15°N) is transmitted into the Celebes Sea and Luzon Strait, whereas approximately two-thirds of the energy is dissipated, transformed, or reflected along the Philippine coast. Approximately 15 % of the energy entering the Celebes Sea passes through the Sibutu Passage into the Sulu Sea, and ~10 % exits the Mindoro Strait into the central SCS. These suggest that 2−5 % of the incident energy from the western North Pacific transmitted into the central SCS and influences sea level and velocity variations there.

1. Introduction

Westward-propagating tropical Rossby waves, which manifest as sea level anomaly (SLA) signals, that impinge on the western boundary of the North Pacific can transmit through straits and passages into the central South China Sea (SCS). The transmission of these waves may significantly influence sea level variability, hydrography, and geostrophic currents around the Philippines Archipelago and SCS (Fig. 1a) from interannual to intraseasonal timescales (e.g., Zhuang et al., 2013; Hu et al., 2022; Jan et al., 2021). The transmission of Rossby waves may generate physical processes that provide substantial biological benefits to the marginal seas of the southern Philippine Archipelago. These processes, such as upwelling and mixing of nutrient-rich subsurface waters with surface waters, can intensify coastal upwellings and, in turn, impact the important regional sardine fisheries in the Bohol Sea and Sulu Sea, as documented by Cabrera et al. (2011) and Villanoy et al. (2011). Furthermore, the transmission of Rossby waves can increase coastal sea levels, thereby increasing the risk of severe damage during storm surges (Calafat et al., 2018). Given the significant role of Rossby waves in affecting the central SCS sea level and velocity variations, managing fisheries, and mitigating coastal risks around the Philippine Archipelago, it is crucial to understand the characteristics of these westward-propagating SLA signals and their subsequent transmission through gateways between islands. Despite its importance, this research topic has rarely been addressed in the open literature and warrants a thorough investigation. Therefore, the objective of this study is to

---

* Corresponding author at: Institute of Oceanography, National Taiwan University, Taipei 106319, Taiwan, ROC
E-mail address: senjan@ntu.edu.tw (S. Jan).

https://doi.org/10.1016/j.pocean.2025.103481
Received 25 October 2024; Received in revised form 4 March 2025; Accepted 17 April 2025

examine the physical processes that occur as Pacific tropical Rossby waves impinge on the western boundary and their links to current velocity variations in the central SCS.

Jan et al. (2021), using a moored 75-kHz acoustic Doppler current profiler (ADCP) deployed in the eastern central SCS from December 2016 to December 2017, supported by satellite SLA in the SCS (Fig. 1b), identified four significant intraseasonal variations in zonal velocities with periods of 50–60 days from May to November 2017 (Fig. 1c). They noted that although velocity oscillations occurred between January and April, their correlations with SLA variability off the Palawan coast were weak (Fig. 1b and 1c). For the four distinct velocity-SLA correlated events, the time and longitudinal variations in satellite altimetry SLAs (Fig. 1b) suggested that these variations were associated with Rossby waves generated by the consecutive rise and fall of coastal sea levels along the western coast of Palawan. For the first three sea level oscillation events shown in Fig. 1b, Jan et al. (2021) attributed these coastal sea level pile-ups and collapses and corresponding Rossby waves emanating from the Palawan coast to the increase and decrease in shoreward Ekman transport, respectively. These fluctuations were induced by the strengthening and weakening of the southwesterly monsoon associated with the boreal summer intraseasonal oscillation (BSISO). These westward-propagating Rossby waves with phase speeds of 0.2–0.3 m s^{-1} in the central SCS, passing through the ADCP mooring, caused these ~ 50-day velocity oscillations. Further analysis suggested that the wave speeds were consistent with the theoretical first mode baroclinic Rossby wave speed of 0.25 m s^{-1} at 10.5°N. In addition to the Ekman transport dynamics, the positive wind stress curl that occurred west of Palawan as the alongshore winds strengthened contributed to the coastal sea level rise observed during the three events. An idealized numerical experiment conducted in their study successfully reproduced the key characteristics observed in the ADCP and satellite data, providing strong support for the dynamic interpretation of the intraseasonal oscillations proposed by Jan et al. (2021).

However, Jan et al. (2021) noted that the correlation between the summer monsoon wind variability and the fourth zonal velocity oscillation event (Os4 in Fig. 1b and c) was weak. Therefore, on the basis of the studies by du Penhoat and Cane (1991) and Spall and Pedlosky (2005), they further hypothesized that SLA signals related to westward-propagating Rossby waves in the tropical North Pacific could transmit through the Philippine Archipelago into the Sulu Sea and eventually into the central SCS, contributing to the observed sea level variations. Moreover, du Penhoat and Cane (1991) and Spall and Pedlosky (2005) demonstrated that when a first-mode baroclinic Rossby wave encountered a small meridional gap in the western boundary, a significant portion of the wave energy can pass through the gap. This theoretical framework supported the hypothesis proposed by Jan et al. (2021). This research has motivated us to carefully examine this hypothesis and the associated SLA energy transmission rate.

Furthermore, this study is motivated by the unique pathway of low-frequency SLA signals through the Philippine Archipelago, as suggested by Zhuang et al. (2013). Focusing on interannual to decadal timescales, Zhuang et al. (2013) examined the impact of long-term SLA variations on sea level and circulation around islands and marginal seas of the Philippines. By using satellite altimeter data and a reduced gravity model, they revealed that westward-propagating baroclinic Rossby waves impinging on the eastern coast of the Philippines generate coastal Kelvin waves, propagating anticyclonically along the coast of the western Philippines. This process enables the SLA signals to enter the Sulu Sea through the Sibutu Passage and to further transmit into the SCS via the Mindoro Strait. Their satellite altimeter data analyses and numerical simulations suggest that SLA variability off the east and west coasts of the Philippines is significantly correlated with climate variations associated with El Niño-Southern Oscillation (ENSO). However, they noted that accurately quantifying energy transmission from east of the Philippines through straits and passages into the SCS would merit future studies that involved more sophisticated numerical models incorporating three-dimensional, nonlinear dynamics, eddy viscosity and diffusivity, and more realistic bathymetry than those used in their reduced gravity model. This approach would verify the coastal Kelvin wave transmission scenario they proposed. Additionally, investigating similar transmission processes for SLA variability on much shorter timescales, such as intraseasonal variations, would be of interest.

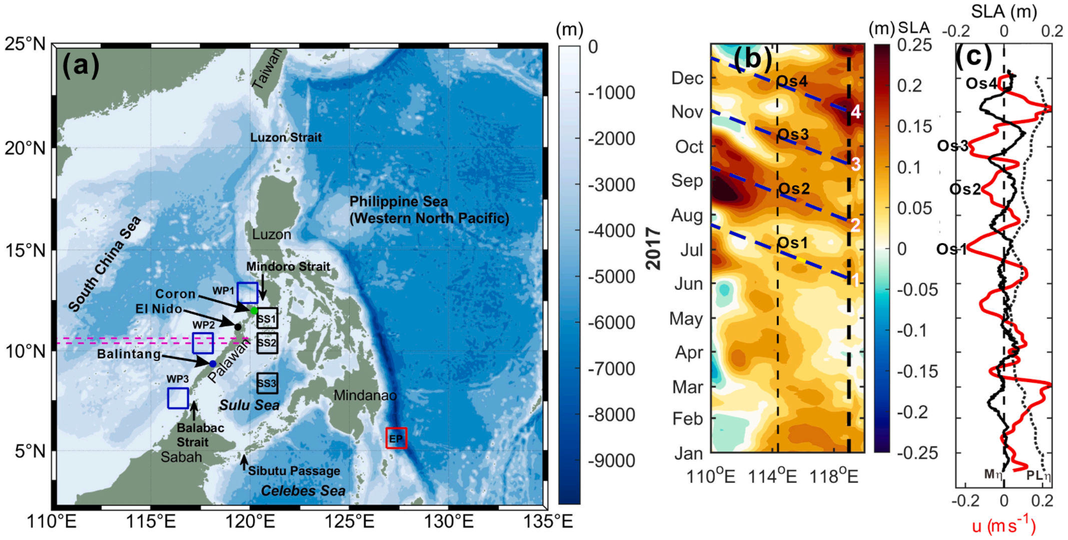

Fig. 1. (a) Bathymetric chart of the Philippine Sea and the South China Sea (SCS). The colored boxes are the selected satellite mean SLA sites located off the east coast of the Philippines (EP), in the Sulu Sea (SS1–3), and off the western Palawan (WP1–3). Coron, El Nido, and Balintang are coastal tide-gauge stations. (b) Longitudinal and time variations in meridionally-averaged satellite SLA at 10.5°N, as indicated by the magenta dashed lines in (a). Numerals 1–4 indicate coastal sea level oscillation events off the west coast of Palawan (black dashed line). The blue dashed lines indicate the best-fit slope of the westward-propagating SLA signals associated with events 1–4 in the central SCS. (c) 8.33-d low-pass-filtered zonal velocity (red line) and sea level (Mη, thick black line) at a location west of Palawan (114.3°E, 10.5°N) from 2016/12/18 to 2017/12/18 (Jan et al., 2021). The low-pass-filtered sea level off the west coast of Palawan is shown by the black dotted line (PLη). Os1–4 indicate the peak westward velocities of the four intraseasonal velocity oscillation events. (For interpretation of the references to color in this figure legend, the reader is referred to the web version of this article.). (For interpretation of the references to color in this figure legend, the reader is referred to the web version of this article.)

Notably, Hu et al. (2022) conducted a similar investigation but focused on ENSO impacts on the Indonesian seas and the connection between the tropical Pacific and Indian Oceans. Their study highlighted the crucial role of ENSO-induced westward-propagating Rossby waves in transporting climate anomaly signals into the Indian Ocean.

Considering aforementioned research, the objective of this study is to investigate the potential dynamic link between sea level and the fourth zonal velocity oscillation event observed in the central-eastern SCS in the summer of 2017 and the westward-propagating tropical Rossby waves that reached the eastern Philippines. The hypothesized transmission process of Rossby waves from the eastern to the western side of the Philippine Archipelago is examined. By analyzing satellite altimeter data and numerical model results, the pathways and arrival times of SLA variations off the east coast of the Philippines, in the Celebes Sea and Sulu Sea, and in the Mindoro Strait at the intraseasonal timescale are identified. The levels of SLA energy transmission are calculated based on model-produced sea level and velocity anomalies. Coastal sea level data from selected tide-gauge stations are analyzed to supplement satellite altimeter observations. The cause for the fourth intraseasonal SLA variation and associated velocity oscillation (marked by "4″ and "Os4" in Fig. 1b and c, respectively), which resulted in a westward-propagating Rossby wave from the west coast of Palawan toward the central-western SCS, is investigated to evaluate the hypothesis by Jan et al. (2021). Section 2 describes the satellite data, sea level measurements from coastal tide-gauge stations, associated measurement errors, and the numerical model. The results and discussion are presented in Sections 3 and 4, respectively, followed by the conclusions.

2. Data and Methods

2.1. Sea level data

The satellite altimeter-derived Global Ocean Gridded (L4) Sea Surface Heights and Derived Variables Reprocessed, provided by the Copernicus Marine Service (available at https://doi.org/10.48670/moi-00148), were collected to identify Rossby waves in the context of sea surface height observations. Note that the Copernicus Marine Service satellite-derived dataset underwent an upgrade on 7 October 2021 (see Quality Information Document, p. 2, #5). Jan et al. (2021) utilized daily SLA data from 2017, prior to this upgrade, whereas our study employs daily SLA data from the improved dataset after the upgrade. This variation in SLA accuracy does not affect the analysis of this study.

The satellite-derived SLA data, with a spatial resolution of 0.25° in both the meridional and zonal directions, were obtained using the standard procedure for deriving the gridded SLA product provided by the Copernicus Marine Service (https://doi.org/10.48670/moi-00148). In this procedure, the climatological mean sea level was calculated over a 20-year reference period (1993–2012) using satellite altimeter data, which were then subtracted from the raw altimeter data to produce the gridded SLA dataset, spanning from 1993 to 2023. This reference period is commonly used to ensure consistency and comparability across datasets. The SLA was estimated by optimal interpolation, combining L3 along-track data from various altimeter missions, by following the method described by Pujol et al. (2016). The processed daily SLAs, particularly those from 2017, were specifically analyzed to validate the hypothesis proposed by Jan et al. (2021) regarding the transmission of intraseasonal Rossby waves through the Philippine Archipelago. Additionally, hourly coastal sea level data recorded at three coastal tide-gauge stations (Fig. 2, locations shown in Fig. 1a) were collected from the National Mapping and Resource Information Authority of the Philippines to supplement the analysis. Since the sea level recorded at the tide-gauge station in Balintang (blue line in Fig. 2b) contained ∼10 % missing data (periods indicated by blue dashed line segments in Fig. 2b), a harmonic analysis was performed using the MATLAB package T_Tide (Pawlowicz et al., 2002) to compute the tidal harmonic constants. These harmonic constants were then used to reconstruct the tidal sea levels during the missing data period.

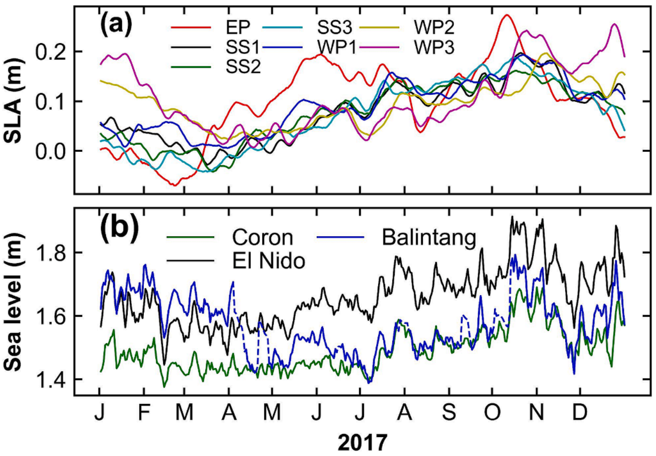

Fig. 2. (a) Time series of the area-averaged daily satellite SLA in 2017 at seven selected rectangular sites (EP, SS1–3, and WP1–3 in Fig. 1a). (b) Time series of the daily-averaged coastal sea level data at three tide-gauge stations, Coron, Balintang, and El Nido along the Palawan coast (locations shown Fig. 1a). The blue dashed line segments indicate data gaps at Balintang. (For interpretation of the references to color in this figure legend, the reader is referred to the web version of this article.). (For interpretation of the references to color in this figure legend, the reader is referred to the web version of this article.)

2.2. Methods

The time series data of the area-averaged daily satellite SLAs at seven selected rectangles (Fig. 1a) were analyzed to evaluate whether the westward-propagating SLA signals could pass through the Philippine Archipelago to the eastern SCS. Three of the seven selected sites are located west of Palawan within the rectangles of 12.375°N–13.375°N and 119.375°E–120.375°E (WP1), 9.875°N–10.875°N and 117.125°E–118.125°E (WP2), and 7.125°N–8.125°N and 115.875°E–116.875°E (WP3). The three sites located in the Sulu Sea are within the rectangles of 11.125°E–12.125°N and 120.375°E–121.375°E (SS1), 9.875°N–10.87°N and 120.375°E–121.375°E (SS2), and 7.875°N–8.875°N and 120.375°E–121.375°E (SS3). The last site is located east of the Philippines (EP) bounded by 5.125°N–6.125°N and 126.875°E–127.875°E. The linear least square fit of each area-averaged daily satellite SLA time series at the seven rectangles was subtracted from its corresponding daily data shown in Fig. 2a to remove the linear trend specific to the SLA variation at each rectangle. This approach ensured that localized linear trends, rather than the globally-averaged trend, were accounted for in our analysis. A similar detrending method was applied to the daily-averaged sea level records at the Coron, Balintang, and El Nido tide-gauge stations.

To investigate the intraseasonal variations in the processed satellite SLAs, the detrended SLA and coastal sea levels were low-pass filtered using a Butterworth filter with a cutoff frequency of 3.8580×10^{-7} cps (equivalent to a period of 30 days). The daily SLA at each 0.25° grid, ranging between 0°–15°N and 110°E–180°E, was also detrended and low-pass filtered through the same procedure. The resulting data were plotted as monthly means to provide a spatial and temporal view of the low-pass filtered SLA variability. This dataset was also used to examine whether the observed SLA signals off the east coast of the Philippines, as discussed in Jan et al. (2021), originated from westward-propagating Rossby waves. The possible transmission route of these waves is also examined by applying the lead and lag correlation analysis to the low-pass-filtered SLA data. To ensure a robust assessment of statistical significance, the Monte Carlo method (Robert and Casella, 2004) was used, which accounted for the reduced degrees of freedom introduced by low-pass filtering. To achieve this, 100 sets of randomly generated errors (Gaussian noise) were added to the shifted time series, and cross-correlation analysis was performed. The random error was generated by sampling from a standard normal distribution and scaling the values by a factor of 0.1. This process was repeated 100 times to obtain a distribution of cross-correlation values. The 95 % confidence interval was then determined by excluding the lowest and highest 2.5 % (approximately 2 % in practice) of the estimated cross-correlation values. A cross-correlation lag was considered significant if it exceeded the bounds of this confidence interval.

The measurement error for the SLA obtained from satellite altimeter data, including with the dataset, was determined by estimating errors in the SLA time series at the central point of each rectangle in Fig. 1a. By using the method described in Pujol et al. (2016), the time series of measurement errors for the seven rectangles were plotted, as shown in Supplementary Fig. S1, for the SLAs in each rectangle. The errors were typically less than 0.02 m across the Philippine Archipelago and ~ 0.01 m west of Palawan. The errors in sea level observed at the tide-gauge stations in Coron, El Nido, and Balintang were derived from the Fourier power spectrum of the sea level data (Fig. S2 in Supplementary). According to the 95 % confidence interval of the power spectrum (Fig. S2), the energy density peak at an intraseasonal frequency of 5.7×10^{-4} cph (equivalent to a period of 73 days) is significant, indicating that intraseasonal variations in the low-pass-filtered sea level data were reliable. The associated error of the coastal sea level observed at Coron, El Nido, and Balintang was approximately 0.03 m, which was the square root of the mean difference between the upper and lower bounds of the 95 % confidence interval.

2.3. Numerical model

The Princeton Ocean Model (Blumberg and Mellor, 1987) was employed to explore the transmission of SLA signals through the Philippine Archipelago and their energetics. The model's governing equations, with the Boussinesq and hydrostatic approximations, consist of three-dimensional, non-linear, primitive momentum equations, a continuity equation, and an equation of state as originally described by Blumberg and Mellor (1987). The governing equations are described in Appendix A. The model topography is established by the ETOPO2v2 bathymetric data (available at https://www.ngdc.noaa.gov/mgg/global/etopo2.html). The model domain was enclosed between the 2°N and 40°N parallels and 100°E and 125°W meridians, encompassing most of the North Pacific. There were no lateral open boundaries in the model. The horizontal grid space was 0.1° between 2°N and 40°N and west of 140°E in the zonal and meridional directions, whereas the grid spacing was 0.2° east of 140°E in the zonal direction. These grid resolutions yielded 876 and 381 grids in the zonal and meridional directions, respectively. The 0.1° (~11 km) horizontal grid resolution was sufficient to resolve major passages and straits in the archipelago while filtering out narrower and less significant passages. For example, Sibutu Passage, Celebes Sea and Sulu Sea, Balabac Strait, and Mindoro Strait have widths of ~ 50, ~50, and ~ 100 km, respectively. These widths were resolved by 4–9 grids in the model, which was adequate to allow SLA signals to pass through. In contrast, most of the passages and straits in the eastern archipelago are narrow, with widths of less than 30 km, and are shallow; thus, these passages and straits were not effective for SLA transmission. The bottom depth of the model topography was set to 6000 m when the depth was greater than 6000 m, which did not influence the physical processes the model produced around the Philippine Archipelago. There were 41 uneven layers in the vertical σ–coordinate. The normalized center depth of each layer is described in Appendix A. A similar numerical model, with various configurations and modeling strategies, has been used to investigate the dynamics of baroclinic tides in the SCS (Jan et al., 2007, 2008), eddy-Kuroshio interactions off Taiwan (Chern et al., 2010; Jan et al., 2017), and intraseasonal oscillation of currents in the central SCS (Jan et al., 2021).

The modeling strategy in this study was focused on the SLA transmission processes and the associated energetics in a relatively "clean" dynamic field without interference from other processes, such as barotropic and baroclinic tides, wind-driven currents, and seasonal hydrographic variations induced thermal/salinity expansion and contraction. The model settings included a simplified initial field and idealized forcing to generate propagating SLA signals. The initial field was set to be motionless for each numerical experiment. An idealized temperature profile and the corresponding density vertical profile (see Appendix A) were given at each horizontal grid to establish a horizontally homogeneous and vertically stratified initial hydrographic field. The salinity was kept constant at 34.5 throughout the simulation.

The Rossby waves in the model were simply generated by wind burst forcing (Anderson et al., 1979; Qiu, 2003; Cabanes et al., 2006), although baroclinic instabilities could generate these waves (Chelton et al., 1998; Cessi and Primeau, 2001; Qiu and Chen, 2004; Mensah and Ohshima, 2020). As in Spall and Pedlosky (2005), a zonal wind stress (detailed in Appendix A) was applied to the sea surface to trigger sea level variations. The wind forcing applied here did not represent realistic wind events but was instead used as a wave generator to create Rossby waves in the model. The model was spun up from rest and ran for 540 days for each experiment. Numerical experiment A (Exp. A hereafter) was the control run, conducted with an easterly wind stress field centered at (6°N, 160°W), a maximum wind stress of$\tau_{max} = 0.2$ N m^{-2}, and an effective wind duration of $T_w = 30$ d from the beginning of the numerical integration. The spatially averaged wind stress over the effective period was 0.127 N m^{-2}, corresponding to a wind speed of 10 m s^{-1}.

Four additional numerical experiments were conducted to investigate the influences of key factors on the transmission of SLA signals and energy flux through the Philippine Archipelago, including the widths and depths of crucial straits/passages, duration of the wind forcing used to generate Rossby waves, wind direction, and the position of wind forcing. In experiment B (Exp. B), the topography around the Sibutu Passage, Balabac Strait, and Mindoro Strait was digitally modified by widening their widths and increasing them to 200 m. The role of these gateways in transmitting SLA energy is evaluated in Exp. B. In experiment C (Exp. C), the effective wind forcing duration was increased from 30 to 60 days to assess how the longer presence of the SLA signal east of the Philippines affected the amount and ratio of energy transmission through the archipelago. The wind direction in experiment D (Exp. D) was reversed from easterly to westerly to generate westward-propagating negative SLAs (trough). This experiment allowed us to compare the differences in energy transmission and pathways between upwelling (trough) and downwelling (crest) Rossby waves. Experiment E (Exp. E) shifts the center of the wind forcing southward, from 6°N to 5°N, to evaluate the influence of the central position of Rossby waves on energy transmission in the archipelago. The temporal and spatial variations in the westward-propagating Rossby waves and their energetics in these experiments were compared across the experiments and with those in the control run (Exp. A). The key parameters used in the control run and each experiment are listed in Table 1.

3. Results

3.1. Satellite SLAs and coastal sea levels

Fig. 3 shows the time series of the detrended and 30-day low-pass filtered satellite SLA and coastal sea levels in 2017. Particular attention is focused on the SLA variations during May and November, as distinct intraseasonal variations in sea level and velocity can be observed in the central-eastern SCS during the summer and fall of 2017 (Jan et al., 2021). The satellite SLA variations at boxes SS1, SS2, and SS3 in the Sulu Sea and WP1, WP2, and WP3 off the west coast of Palawan are significantly correlated with the coastal sea level variations at Coron, Balintang, and El Nido. These correlations suggest that the SLA

Table 1
Model settings in the control run (Exp. A) and each numerical experiment. τ_{max} is the maximum amplitude of the wind stress, (x_0, y_0) is the center position of the wind forcing, and T_w is the effective duration of the wind stress applied to the sea surface.

Exp.	τ_{max}(N m^{-2})	x_0, y_0	T_w (days)	Topography
A	0.2	6°N, 160°W	30	ETOPO2v2
B	0.2	6°N, 160°W	30	Sibutu Passage (119.3–120.7°E, 5.0–6.0°N), Balabac Strait (116.7–117.7°E, 7.5–8.5°N), and Mindoro Strait (119.8–121.4°E, 10.5–11.7°N) and (119.2–120.8°E, 11.8–12.7°N) were digitally widened and deepened to 200 m.
C	0.2	6°N, 160°W	60(Wind duration doubled)	ETOPO2v2
D	–0.2(Wind direction reversed)	6°N, 160°W	30	ETOPO2v2
E	0.2	5°N, 160°W(Wind fetch center shifted 1° southward)	30	ETOPO2v2

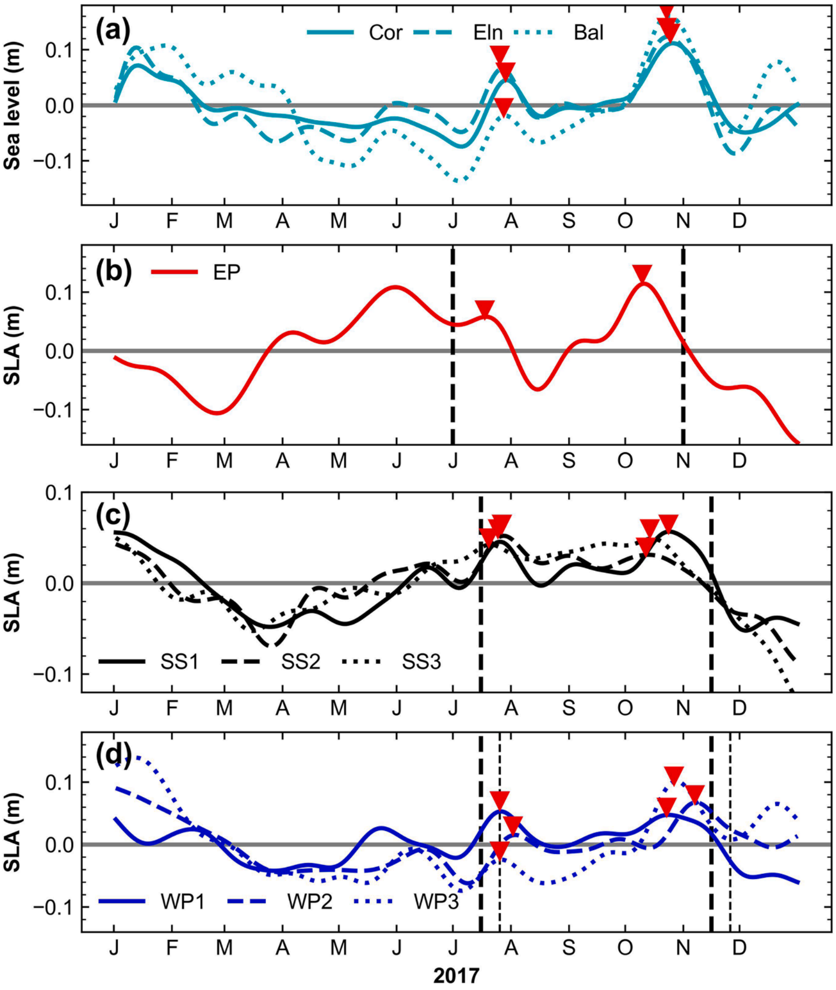

Fig. 3. (a) Time series of detrended and 30-day low-pass filtered coastal sea levels recorded at (a) the west and north coasts of Palawan, and satellite SLAs at (b) the east coast of the Philippines EP, (c) the Sulu Sea SS1–3, and (d) the west coast of Palawan WP1–3. The abbreviations Cor, Bal, and Eln indicate Coron, Balintang, and El Nido, respectively. The time span between the two thick vertical dashed lines in (b), (c), and (d) represents the duration of the positive SLA signal (crest), and that between the two thin vertical dashed lines in (d) represents the duration of the positive SLA signal (crest) at WP2. Red inverse triangles mark SLA peaks at each location during July and December 2017. (For interpretation of the references to color in this figure legend, the reader is referred to the web version of this article.). (For interpretation of the references to color in this figure legend, the reader is referred to the web version of this article.)

variations captured by these coastal tide-gauge stations are presented in the 1° × 1° box-averaged satellite data. Therefore, the satellite SLA data at these locations can be a proxy for representing coastal sea level variations.

Fig. 3b shows two associated peaks with SLA amplitudes of 0.06–0.12 m occurring at EP in 17 July and 9 October 2017 (as indicated by the red inverse triangles in Fig. 3). Fig. 3c shows that similar SLA peaks in the Sulu Sea with lower amplitudes of 0.04–0.06 m can be observed in 19–26 July and around 11–23 October, and west of Palawan (0.06–0.10 m) around 25 July at WP1 and 22–26 October at WP1 and WP3 (Fig. 3d). The SLA peaks at WP2 (0.02–0.06 m) appear on 1 August and 6 November, ~10 days after those at WP1. WP3 is located off the Balabac Strait, which connects the Sulu Sea to the central SCS (Fig. 1a). When the SLA signal enters the Sulu Sea, a small fraction of its energy can transmit through the Balabac Strait (Fig. 1a), despite its limited width (~50 km) and depth (~100 m), and causes SLA variations at WP3 that lead those at WP2. The observed lead and lag correlations in Fig. 3d are consistent and reasonable in this context.

Significant intraseasonal SLA variation at EP occurred between 1 July and 1 November (within the two thick vertical dashed lines in Fig. 3b). At SS1, SS2, and WP1, this significant variation begins ~ 15 days later, from mid-July to mid-November. At WP2, significant SLA variation can be observed from late July to late November (indicated by thin vertical dashed lines in Fig. 3d), ~10 days after the variations at SS1, SS2, WP1, and WP3. The lagged correlation coefficient (r_{SLA}) values between the SLA variations in the Sulu Sea (SS1–2) and off the eastern Philippines (EP) are in the range of 0.5–0.6, with a lag of 12–17 days. The r_{SLA} between the SLA variation off the western Philippines (WP2) and in the northern Sulu Sea (WP1 and SS1) is 0.5–0.7, with a lag of 8–10 days. These correlation coefficients are above the 95 % confidence level.

According to the findings from Fig. 3 and the lagged correlation analysis, the coherent SLA signals off the eastern Philippines lead those in the Sulu Sea by ~15 days, whereas SLA signals in the Sulu Sea lead those off western Palawan by ~ 10 days. This finding supports the hypothesis proposed by Jan et al. (2021). Notably, the variability in propagation timing can be attributed to the complex topographic features and coastal geometries within the archipelago, which influence the transmission and dispersion of SLA signals. The narrow pathways and shallow depths between SS1 and WP1 (despite their geographic proximity) can reduce the speed of the propagating SLA signal.

A map of monthly satellite SLAs from the SCS to 180°E in Fig. 4 is used to help identify the possible spatial and temporal coherence of the intraseasonal SLA signals. Fig. 4a shows a negative SLA region off the eastern Philippines, followed by a zonally extended positive SLA signal along ~5°N. In April, the leading edge of the positive SLA signal, with its primary crest (indicated by a black open oval in Fig. 4b) located roughly between 132°E and 140°E, reaches the east coast of the Philippines (Fig. 4b). The primary positive SLA crest impinges on the Philippine Archipelago from May to July (Fig. 4c–e), and then dissipates until August (Fig. 4f). As the positive SLA fades, weak negative SLAs reach the Philippines along the direction 5°N in August and September (Fig. 4f and 4 g). The wave speed, estimated from Fig. S3 in Supplementary, is ~0.68 m s^{-1}, comparable to the theoretical first-mode baroclinic Rossby

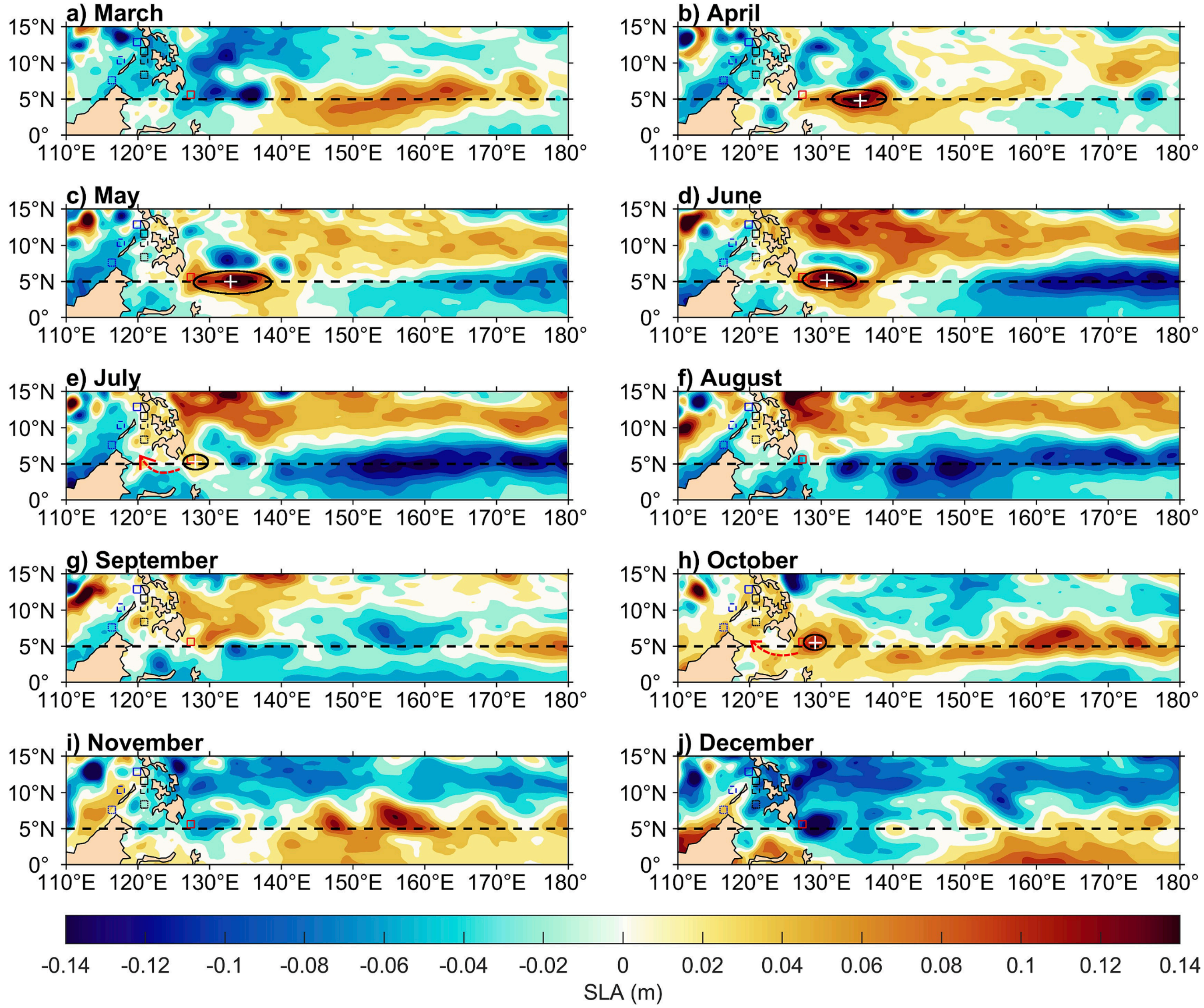

Fig. 4. Monthly temporal and spatial variations in the detrended and 30-day low-pass filtered satellite SLAs in 2017. The black open ovals indicate the peak positive SLA (marked by white "+") areas along 5°N. The red dashed lines in (e) and (h) represent the possible transmission routes of the SLA crest. The color and line style of the rectangles correspond to those shown in Fig. 3b–d. (For interpretation of the references to color in this figure legend, the reader is referred to the web version of this article.). (For interpretation of the references to color in this figure legend, the reader is referred to the web version of this article.)

wave speed (0.7 m s^{-1}) and model-derived phase speed of Rossby waves at 5°N (0.67 m s^{-1}; Kessler, 1990).

A pair of westward-propagating SLA crests and troughs appears at relatively high latitudes between 10 and 15°N from June to December, as shown in Fig. 4d–j, and in a longitude–time plot of detrended and 30-day low-pass filtered daily SLAs centered at 10.5°N (averaged between 10.375°N and 10.625°N) from 130°E to180°E (Supplementary Fig. S4). The wave speed, estimated from Fig. S4, is ~0.28 m s^{-1}, which is consistent with the first-mode baroclinic Rossby wave speed estimated by Chelton and Schlax (1996) and that observed by Jan et al. (2021) in the central SCS. However, these SLA signals at higher latitudes are less likely to transmit into the Celebes Sea or pass through the archipelago into the central SCS than those at lower latitudes.

As a positive SLA crest located at 5–6°N approaches the east coast of the Philippines in July (indicated by a black open oval in Fig. 4e), it may subsequently propagate into the Celebes Sea and Sulu Sea, as suggested by the red dashed arrow in Fig. 4e. One month later, in August and September, an SLA trough reaches the eastern Philippines (Fig. 4f and 4 g), followed by a new positive SLA crest in October (Fig. 4h). This positive SLA likely evolved from the northeast, as suggested by Fig. 4g. Regardless of its exact origin, this SLA represents a key feature in early October for subsequent transmission through the Philippine Archipelago into the central SCS by mid-November 2017. This inference can be supported by coherent SLA peaks of ~0.06 m at SS1–3 (late July in Fig. 3c) and at WP1 (Fig. 3d). The SLA peak subsequently propagates toward WP2 with a value of ~ 0.02 m (early August in Fig. 3d) ~10 days after passing WP1.

The 0.02 m SLA peak at WP2 propagates westward, partially contributing to the second SLA event (Fig. 1b) observed by Jan et al. (2021). The SLA at WP2 then decreases in September (Fig. 4g and 3d). The trailing SLA crest continues to propagate toward WP2 in October (Fig. 4h) and November (Fig. 4i). In November, the SLA crest (Fig. 4i) apparently passes WP1 (Mindoro Strait), leading to a 0.06 m SLA peak in early November (Fig. 3d). This SLA signal eventually reaches WP2 (Fig. 3d) and further propagates westward, contributing to the fourth event ("4" in Fig. 1b and Os4 in Fig. 1c) observed by Jan et al. (2021).

3.2. Numerical results of the control run

The maximum wind stress at day 15 in Exp. A is shown in Fig. A1. The wind stress induces various frequency SLA variations during the forced period, which encompasses the first 30 days of numerical integration. The model-produced sea level variations show that higher frequency, fast-moving positive SLA crest acting as a gravity wave, reaches the east coast of the Philippines and enters the Celebes Sea at lower latitudes within the first tens of days (not shown). After the forced period, the modeled wind-induced SLAs and the corresponding velocities at a 20 m depth at model days 60, 90, 120, 150, 180, 210, 240, and 270 are shown in Fig. 5.

Fig. 5a shows a positive sea level crest, at an order of magnitude greater than 0.01 m in height and extending 5000 km (~45 degrees) in the zonal direction moving westward at day 60. Wind-induced SLAs with different translation speeds cause the primary positive sea level crest to be continuously elongated westward over time. There are eastward-propagating negative (or trough) SLAs, which are typically categorized as equatorial Kelvin waves (e.g., Battisti, 1989; Giese and Harrison, 1990; Webber et al., 2011). During the forced period and approximately 30 days afterward, SLA signals reaching east of the Philippines can be dominated by first-mode baroclinic gravity waves with phase speeds of ~3 m s^{-1} (Chelton et al., 1998), traveling a distance of ~7000 km. Regardless of these fast-moving SLA signals, we focused on the positive SLA signals (SLA ≥ 0.01 m) after day 60 for the

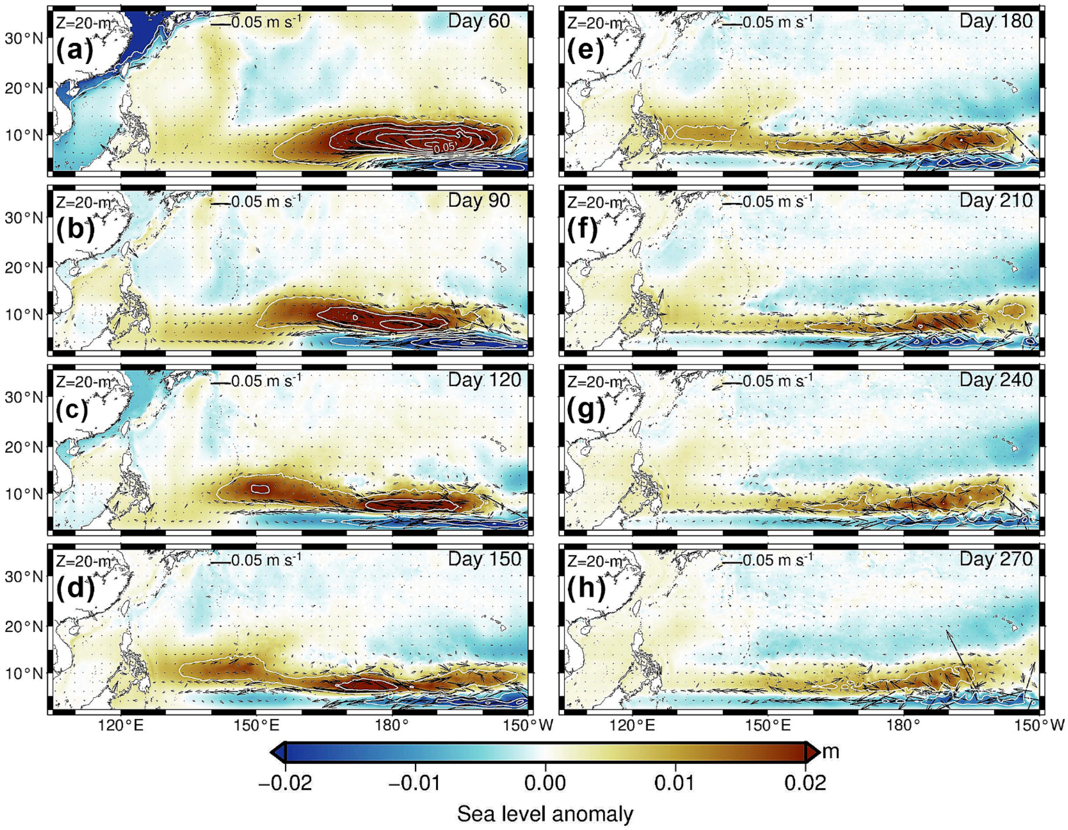

Fig. 5. Model-produced instantaneous sea level (color shading) and velocity (arrows at 20 m depth) for numerical experiment A at days (a) 60, (b) 90, (c) 120, (d) 150, (e) 180, (f) 210, (g) 240, and (h) 270. Sea level anomaly contour is at intervals of 0.01 m. Velocity arrows are plotted every 2° in both the zonal and meridional directions in each panel.

analysis. As shown in Fig. 5b, the leading (western) edge of the freely propagating SLAs, delineated by the 0.01 m contour and with phase speeds of ~0.6 m s^{-1} (consistent with the theoretical first-mode baroclinic Rossby wave, Chelton and Schlax, 1996) approaches the Philippines around day 90, starting to cause a sea level rise in the Celebes Sea, Sulu Sea, and central-northern SCS. At approximately day 150, the leading edge of the positive SLA impinges on the east coast of the Philippines (Fig. 5d) and eventually dissipates by day 240 (Fig. 5g). Therefore, we select the distinct SLA variations during this period (days 120–270) to analyze the pathways and energetics of Rossby wave transmission. In addition to illustrating the SLA variability, Fig. 5 shows that the modeled velocities at the 20 m depth layer are predominantly geostrophic currents.

The westward propagation of model-produced SLAs is demonstrated as the longitude-time plot of sea levels along 5°N, 8°N, and 10°N in Fig. 6. Despite the initial forced, fast-moving gravity waves during the first 60 days, the leading crest of the positive SLA along 5°N reaches the eastern opening of the Celebes Sea from days 100 to 120 (Fig. 6a), causing the sea level to rise in the Celebes Sea. The propagation speed, estimated from the slope of the corresponding SLA signal, decreases from 1.01 m s^{-1} to 0.25 m s^{-1} west of 132°E. A negative SLA trough following the SLA crest at 5°N reaches the Celebes Sea around day 180 (Fig. 6a). Approximately 50–60 days later, the SLA crest (referred to as the western SLA crest in Fig. 5c), propagating westward at a mean zonal speed of 0.61 m s^{-1} at 8°N and 0.45 m s^{-1} at 10°N, impinges on the Philippines' east coast from day 160 to 210 (Fig. 6b and 6c). It takes ~5 − 10 days for the SLA signal from 8°N off the eastern Philippines into the Sulu Sea (Fig. 6b) and ~10 − 15 days from 10°N to reach the Sulu Sea (Fig. 6c).

To examine the coherence and time delays of the model-produced sea level at the locations of the seven rectangles shown in Fig. 1a, the time series of the daily sea level at the corresponding model grids are depicted in Fig. 7 and compared with those in Fig. 3. The time series of sea level at the model grid at 132°E and 10°N (orange line of 132°E in Fig. 7) and three additional locations in the Celebes Sea (green lines of CS1–3 in Fig. 7) are shown as well. Although the amplitude of the modeled SLA signals around the Philippines is smaller than that derived from satellite and tide-gauge observations (Fig. 3), this underestimate does not affect the fundamental physics of SLA signal transmission. The SLA peaks across different regions between days 70 and 100 in Fig. 7 correspond to the propagation of Rossby waves at relatively fast speeds (~0.6 m s^{-1}) at latitudes of ~ 3–6°N (Fig. 5a and 5b). Analysis of these SLA peaks suggests that the sea level peak at 132°E leads that at EP by 8 days, that at EP leads that at SS3 and SS1 by 10 and 20 days (12–17 days in observations), respectively, and that at SS1 leads that at WP2 by ~8 days (8–10 days in observations), consistent with the arrival timing

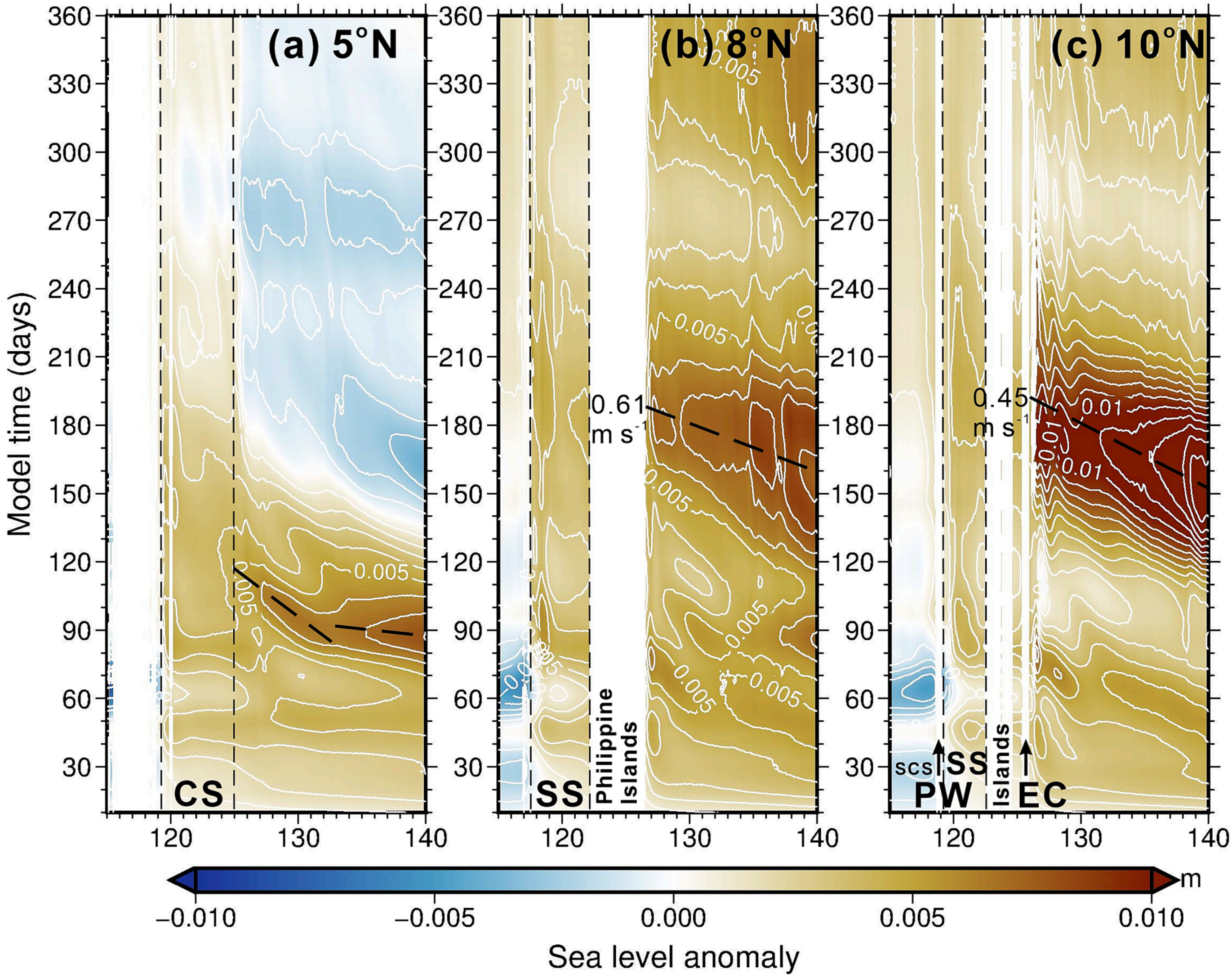

Fig. 6. Time-longitude variation in model-produced sea level (color shading) for numerical experiment A along (a) 5°N, (b) 8°N, and (c) 10°N. CS, SS, PW, and EC denote the locations of Celebes Sea, Sulu Sea, Palawan, and the east coast of the Philippines, respectively, at each latitude.

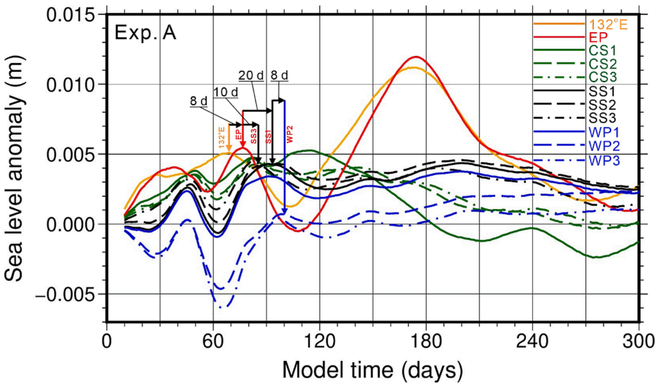

Fig. 7. Time series of model-produced daily SLA at locations corresponding to the rectangles EP (red), SS1–3 (black), and WP1–3 (blue) in Fig. 1. CS1, CS2, and CS3 (green) are located in the eastern opening, central, and western parts of the Celebes Sea, respectively; 132°E (orange) is located at (132°E, 10°N). (For interpretation of the references to color in this figure legend, the reader is referred to the web version of this article.). (For interpretation of the references to color in this figure legend, the reader is referred to the web version of this article.)

derived from the satellite SLA variations shown in Fig. 3.

Following these leading SLA signals, subsequent SLA signals propagate slower (~0.45 m s^{-1}) at higher latitudes of ~5–12°N with more pronounced SLA variation (>0.01 m), reaching the east coast of the Philippines around days 150–180 (Fig. 5d–f). Our analysis of SLA energetics is focused on these pronounced SLA signals propagating from the east between days 100 and 300. Notably, these later SLA signals split into northward- and southward-propagating branches along the east coast of the Philippines, dissipating their influence on SLA variations in the Celebes Sea and Sulu Sea. Moreover, the absence of a corresponding SLA peak in other regions around day 180 in Fig. 7 is attributed to the influence of an accompanying negative SLA signal south of the positive SLA, particularly in the Celebes Sea after day 150 (Fig. 5d). This interaction reduces the contrast of the positive SLA signal in the Sulu Sea, as shown in Fig. 7. Despite the ambiguity in SLA peaks, the time–space variation in SLA energy flux shown later in Fig. 8 provides a comprehensive view, clearly delineating the energy transmission and pathways across the key regions.

3.3. Energetics of the control run

Energy flux is a useful parameter for tracking wave propagation and pathways. The energy flux (or pressure work) of a Rossby wave is defined as the product of the perturbation pressure (p') and horizontal ageostrophic velocity $\boldsymbol{u}_{ag}$ (Cai and Huang, 2013; Durland and Farrar, 2020) as

$$\vec{\boldsymbol{F}} = p'\vec{\boldsymbol{u}}_{ag} \tag{1}$$

where $p' = \rho_0 g\eta$ (η is the sea surface height anomaly and ρ_0 is the initial density profile) and $\vec{\boldsymbol{u}}_{ag} = \vec{\boldsymbol{u}} - \vec{\boldsymbol{u}}_g$ is from the modeled velocity $\boldsymbol{u}$ and geostrophic velocity $\boldsymbol{u}_g$. The ageostrophic velocity is thus derived as $\vec{\boldsymbol{u}}_{ag} = -\frac{1}{\rho_0 f^2}\nabla_H \frac{\partial p}{\partial t}$ (Cai and Huang, 2013), where f is the Coriolis parameter and the operator $\nabla_H = \frac{\partial}{\partial x}i + \frac{\partial}{\partial y}j$. It is important to note that the energy flux associated with geostrophic currents, $p'\vec{\boldsymbol{u}}_g$, is nondivergent and does not relate to the propagation of Rossby waves (Cai and Huang, 2013; Durland and Farrar, 2020).

Computed using Eq. (1), Fig. 8 presents the instantaneous energy fluxes, velocities at a 20 m depth, and SLAs at different days for Exp. A. In Fig. 8a, the first westward-propagating SLA crest at a lower latitude of approximately 5°N establishes an energy flux pathway that flows northward from the Celebes Sea, through the Sibutu Passage, along the western boundary of the Sulu Sea, and into the Mindoro Strait, connecting the Sulu Sea with the SCS. After the forced period, the leading edge of the primary SLA crest, centered at ~ 10°N, impinges on the Philippines' east coast by day 135 (Fig. 6c). By day 150, Fig. 8c shows that the energy flux bifurcates at ~ 10°N off the eastern Philippines: one branch moves northward toward the Luzon Strait, whereas the other moves southward toward the Celebes Sea. This energy flux divergence is influenced by the coastal geometry, bathymetric constraints, and redistribution of energy along the boundary. Note that the energy flux represents wave energy propagation rather than phase propagation of the wave itself. Fig. 8c shows that the northward-moving energy flux in the western Celebes Sea passes through the Sibutu Passage into the Sulu Sea and then follows the east coast of Palawan to the Mindoro Strait. A positive SLA bump forms off the west coast of Luzon Island (indicated by the open arrow in Fig. 8c). This pattern of energy flux propagation around the Philippine Archipelago intensifies and peaks at day 180 (Fig. 8d). The coherent SLA bump off Luzon continues to extend westward. Thereafter, the energy flux around the Philippines weakens (Fig. 8e and 8f), but the SLA bump established off the coast of Luzon around day 150 continuously extends toward the western SCS.

The time series of depth- and section-integrated energy fluxes across each section (location shown in Fig. 8a) are calculated by $\vec{\boldsymbol{F}}_{sec} = \int_{l_1}^{l_2}\int_{-H}^{\eta}\vec{\boldsymbol{F}}\,dzdl$, where l_1 and l_2 are the start and end positions of the sectional integration, respectively. Fig. 9 shows the time variations in the depth-integrated energy flux across the six sections. Fig. 9a shows that the westward energy flux in the 132°E section (location shown in Fig. 8a), integrated from 2°N to 15°N, begins to increase around day 100, peaks at day 165, and significantly decreases after day 200. Notably, the 132°E section is selected to calculate the incident wave energy east of the Philippines. Fig. 9b provides a closer view of the depth-integrated energy flux at the Celebes Sea (CB), Sibutu Passage (SB), Mindoro Strait (MD), Balabac Strait (BB), and Luzon Strait (LZ) sections. This figure shows that ~ 20 days after the peak energy flux at the 132°E section, the energy fluxes at the CB and SB sections peak. Approximately 5–10 days after the peak energy fluxes at the two sections, the energy flux at the MD section peaks. The energy flux through the BB remains relatively weak throughout the integration process. The westward energy flux at the LZ section begins to increase from day 145, lagging ~ 20 days behind the CB section. Fig. 9 indicates that significant variations in the depth-integrated energy fluxes in the six sections occur primarily between days 120 and 300.

The energy across a section during a certain period is computed by $E_{sec} = \int_{t_1}^{t_2}\vec{\boldsymbol{F}}_{sec}dt$, where t_1 and t_2 are the start and end times of the time integration, respectively. With this formula, the energy transmitted through these sections from day 120 to 300 is calculated by integrating the depth-integrated energy flux over this 180-day period. The estimated energy values are subsequently used to calculate the nondimensional energy transmission rate. Table 2 lists the ratios (in percentages) of energy transmitted through the CB and LZ sections relative to the 132°E section (between 2°N and 15°N), and through the SB and MD sections relative to the CB section (locations shown in Fig. 8a). In Exp. A, 20 % of the energy from the westward-propagating SLA crest passing through the 132°E section enters the Celebes Sea along the east coast of the Philippines, whereas 14 % enters the northern SCS via the Luzon Strait. In the Celebes Sea, 16 % of the energy is transmitted through the Sibutu Passage to the Sulu Sea, and 12 % is transmitted through the Mindoro Strait to the central SCS. This result indicates that 78 % of the energy entering the Sulu Sea from the Sibutu Passage (MD/SB in Table 2) is further transmitted through the Mindoro Strait to the central SCS. Approximately 34 % of the energy passing through the 132°E section enters the Celebes Sea and northern SCS, suggesting that approximately 66 % of the incident energy must be dissipated, transformed, scattered, or reflected at the western boundary. Only 2 % of the

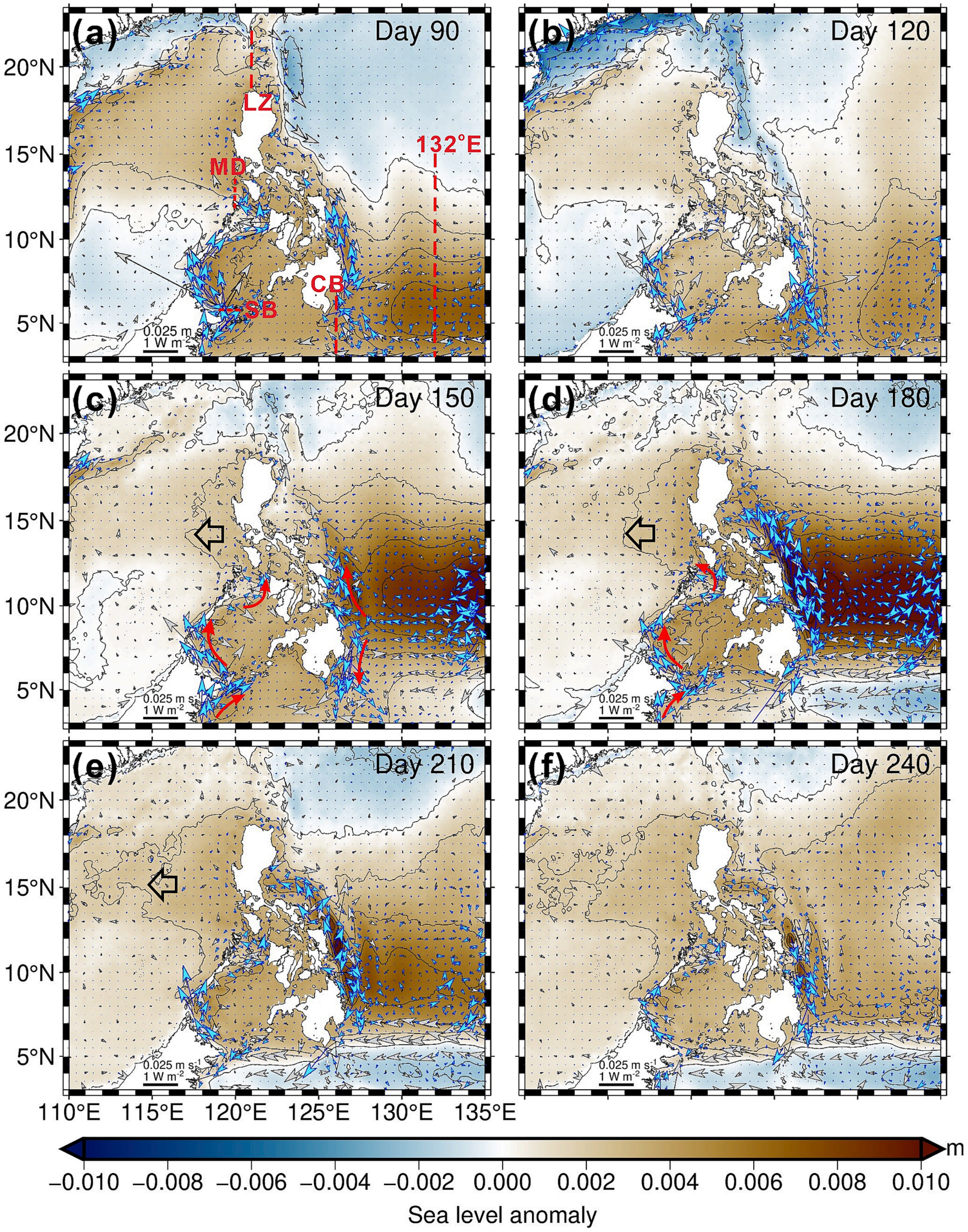

Fig. 8. Model-produced instantaneous sea level (color shading), velocity at a 20 m depth (gray arrows), and energy flux (cyan arrows) for Exp. A at days (a) 90, (b) 120, (c) 150, (d) 180, (e) 210, and (f) 240. The red dashed lines in (a) represent the meridional section at 132°E, across the eastern opening of the Celebes Sea (CB), the zonal section across the Sibutu Passage (SB), the Mindoro Strait (MD), and the meridional section across the Luzon Strait (LZ). The red arrows indicate the moving directions of the energy flux. (For interpretation of the references to color in this figure legend, the reader is referred to the web version of this article.). (For interpretation of the references to color in this figure legend, the reader is referred to the web version of this article.)

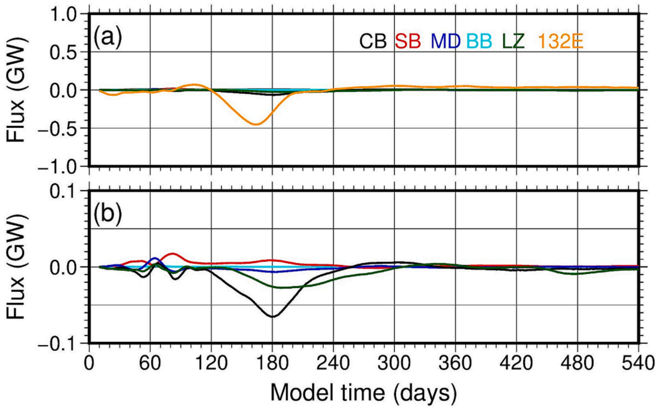

Fig. 9. (a) Time-varying depth-integrated energy flux ($\vec{F}_{sec}$) across the 132°E, CB (Celebes Sea), SB (Sibutu Passage), MD (Mindoro Strait), BB (Balabac Strait), and LZ (Luzon Strait) sections (locations shown in Fig. 8a). (b) Close-up of the energy flux from (a), excluding the 132° section.

Table 2
Estimated ratio of energy transmitted through the CB (Celebes Sea), LZ (Luzon Strait), SB (Sibutu Passage), and MD (Mindoro Strait) sections (locations shown in Fig. 8a) relative to that transmitted through the 132°E (between 2°N and 15°N) and CB sections from day 120 to day 300.

Exp.	Proportion of energy transmission (%)					
	CB/132°E	LZ/132°E	SB/CB	MD/CB	MD/SB	MD/132°E
A	20	14	16	12	78	2
B	22	14	18	5	27	1
C	22	17	17	13	78	3
D	17	7	4	4	87	1
E	31	18	33	15	48	5

incident energy from the 132°E section (MD/132°E in Table 2), following the Celebes Sea-Sibutu Passage-Sulu Sea pathway, ultimately enters the central SCS via the Mindoro Strait.

3.4. Numerical results

Fig. 10 shows the model-produced instantaneous SLA, velocity at a 20 m depth, and energy fluxes for Exps. B, C, D, and E. Moreover, the section- and depth-integrated energy fluxes across the six sections (Fig. 8a) of the four experiments are depicted in Fig. 11. Compared with the map of energy flux in Fig. 8d, both the deepening and widening of straits and passages in the western Philippines in Exp. B considerably enhance the transmission of SLA signals and associated energy from the Sulu Sea to the central SCS, particularly through the widened Balabac Strait (Fig. 10a and 11a). Fig. 10a shows that the transmitted SLA results in coastal sea level rising from not only the Mindoro Strait but also the Balabac Strait. Both sea level rises extend farther from the west coast of Palawan to the western SCS. The energy transmission ratios of the Balabac Strait (location shown in Fig. 1a) and the Celebes Sea significantly increase to 4 % of the energy entering the Celebes Sea. This ratio suggests that ~1 % of incident wave energy can transmit through the Balabac Strait into the central SCS, which is comparable to that through the Mindoro Strait (Table 2). In contrast, the energy transmitted through the Mindoro Strait considerably decreases to 5 %, whereas it decreases to 12 % in Exp. A (Table 2). Compared with the value of 78 % in Exp. A, only 27 % of the energy passing through the Sibutu Passage exits the Sulu Sea via the Mindoro Strait (Table 2).

In Exp. C (Fig. 10b and 11b), the most notable yet unsurprising differences from Exp. A are the remarkable increases in the magnitudes of the SLAs and associated energy flux as the westward-propagating SLA reaches the Philippine Archipelago. The peak energy fluxes passing through the 132°E section lags by ~15 days compared with that in the other experiments. However, the patterns of the energy flux pathways and the levels of energy transmission in this experiment (Table 2) are similar to those in Exp. A (Fig. 8d).

In Exp. D, Fig. 10c shows that the impingement of the westerly wind-induced westward-propagating negative SLA (trough) leads to a sea level decrease in the Sulu Sea and the central SCS, similar to the distribution pattern of positive SLA in Exp. A (Fig. 8d). The energy flux pathways off the east coast of the Philippines and within the Celebes and Sulu Seas resemble those in Exp. A, but the ratios of energy transmission generally decrease compared with those in the other experiments (Table 2, Fig. 11c).

As the center of the wind forcing is shifted 1° latitude southward in Exp. E, the SLA crest of the Rossby waves impinges at more southerly latitudes (Fig. 10d). The most significant result is an increase in the energy from the incident SLA energy entering the Celebes Sea (31 % compared with 20 % in Exp. A, Table 2). The amounts of energy transmitted from the Celebes Sea through the Sibutu Passage (SB/CB) and the associated SLA energy transmitted into the central SCS (MD/132°E) approximately double compared with those in Exps. A, B, and C (Table 2, Fig. 11d). Conversely, shifting the wind forcing center northward results in the SLA signal impinging on the east coast of the Philippines at higher latitudes, which reduces the SLA energy flux transmitted through the Celebes Sea and Sulu Sea pathways. For example, when the wind forcing center is shifted 2° northward to (8°N, 160°W), the energy flux off the eastern Philippines at day 150 is mostly deflected to the north, with a much weaker energy flux entering the Sulu Sea than that in Exp. A. (cf. Fig. S5 in Supplementary and Fig. 8c). While this finding highlights the sensitivity of energy transmission to the location of wind forcings, a more detailed investigation into this scenario merits future study.

In a similar study using a shallow water equation model, Spall and Pedlosky (2005) reported that only 10 % of the incident Rossby wave energy from the western tropical Pacific transmits into the Indian Ocean. This transmission rate is consistent with that derived from a linear theory framework by Clarke (1991). Compared with these studies, the 2–5% energy transmission rate derived from our model experiments appears to be reasonable.

4. Discussion

The specific intraseasonal SLA oscillation and the associated westward-propagating Rossby wave observed by the ADCP in the central-eastern SCS during late summer 2017 (Jan et al., 2021) are selected for considerations in the process study here. On the basis of the results of the aforementioned numerical experiments, similar Rossby wave transmission through the Philippine Archipelago and its influence on central SCS circulation can occur year-round. However, the transmission of Rossby waves in this region may be dissipated, mixed, or smeared by the influence of East Asian monsoon winds, distinct baroclinic tides and internal solitary waves in the Sulu Sea (Apel et al., 1985; Tessler et al., 2012), and seasonal thermal expansion and contraction. Therefore, Rossby wave transmission signals may not be detected by satellite altimeters or coastal tide-gauges. This transmission depends on the strengths of the transmitted SLA signals as well.

Compared with the pathway of the transmitted SLA signals described by Zhuang et al. (2013), although at different timescales, the energy flux obtained in this study indicates that the SLA energy follows the western boundary of the Sulu Sea, rather than the eastern boundary described by Zhuang et al. (2013) after entering through the Sibutu Passage. We quantify the SLA energy transmission rates across the entrances of the Celebes Sea, Sibutu Passage, and Mindoro Strait, based on the incident energy across a meridional section (132°E, 2°N–15°N) before the westward-propagating Rossby waves reach the Philippine coast. By tracking the instantaneous SLA energy flux, we identify the energy pathways from east of the Philippines to the central SCS. In the central-

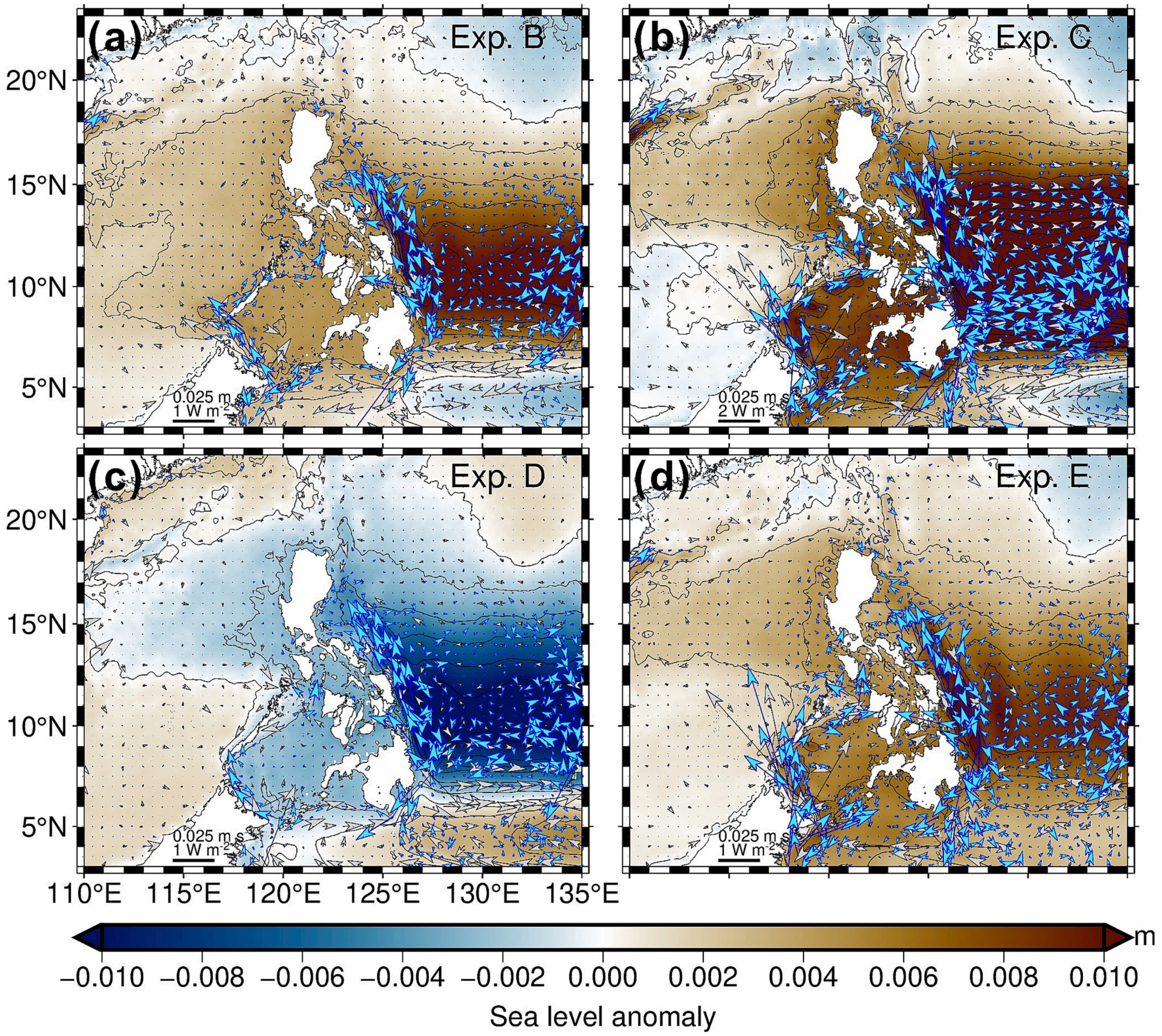

Fig. 10. Same as Fig. 8 but for Exps. (a) B, (b) C, (c) D, and (d) E at day 180. Note that the energy flux scale in (b) is twice that of the other three.

eastern SCS, alongside the intraseasonal SLA variations induced by summer monsoon oscillations off the west coast of Palawan in 2017, the results of this study support the mechanism for intraseasonal SLA oscillations proposed by Jan et al. (2021).

As the transmitted SLA signal passes through the Sibutu Passage into the Sulu Sea, northward-flowing coastal currents along the east coast of Palawan induce coastal upwellings, particularly off the northeast coast of Sabah (not shown). Off the west coast of Palawan, the release of the transmitted positive SLA can generate westward-propagating Rossby waves in the central SCS (Jan et al., 2021), which could further contribute to the intraseasonal variation of the offshore jet off Vietnam (Xie et al., 2007). Conversely, the influence of the SCS currents on oceanic conditions southeast of the Philippines has been examined by Li et al. (2021). Several studies (Li et al., 2021; Gordon et al., 2012; Wei et al., 2016; Li et al., 2019) have examined the role of the Mindoro Strait–Sibutu Passage pathway in facilitating brackish water intrusion into the Celebes Sea, which may control the annual variability of the Indonesian Throughflow. Moreover, the SCS currents flowing through the Mindoro Strait and exiting via the Sibutu Passage can alter the bifurcation point of the North Equatorial Current, thereby affecting the strength of both the Mindanao Current and the Kuroshio (Metzger and Hurlburt, 1996; Li et al., 2021).

The potential biological effects induced by the upwellings may benefit local fisheries. Additionally, eastward-propagating Kelvin waves generated from Rossby wave reflection at the Philippines' east coast are not clear in our numerical experiments. The highly irregular and fractured coastline combined with bottom friction, and horizontal/vertical dissipation in the model can weaken the reflection of model-produced Rossby waves. The investigations by du Penhoat and Cane (1991) and Spall and Pedlosky (2005) may explain the weak reflection of Rossby waves. They have suggested that a significant portion of the westward-propagating Rossby wave's energy can pass through a small meridional gap in the western boundary. Consequently, the reflected Kelvin waves are weakened, potentially impacting ENSO variability in the Pacific Ocean. Alternatively, based on the analysis of satellite sea level data, Zang et al. (2002) indicated that Rossby waves with periods shorter than 180 days are relatively weak and are thus less likely to reflect intraseasonal Kelvin waves; Cravatte et al. (2004) reported the same findings for periods shorter than 100 days. Moreover, Cravatte et al. (2004) found that the reflection of 120-day Rossby waves at the western boundary significantly contributes to the 120-day Kelvin waves observed by satellite altimeters in the tropical Pacific Ocean. To generate significant Kelvin waves from the Philippines' coast, the wind forcing period and wind stress strength in the model can be easily increased; however, this action is beyond the scope of the current study.

In reality, the characteristics of wind-induced SLAs are influenced by the spatial patterns and temporal variations in wind, ocean stratification, ambient circulation, and topography, which are more complex in

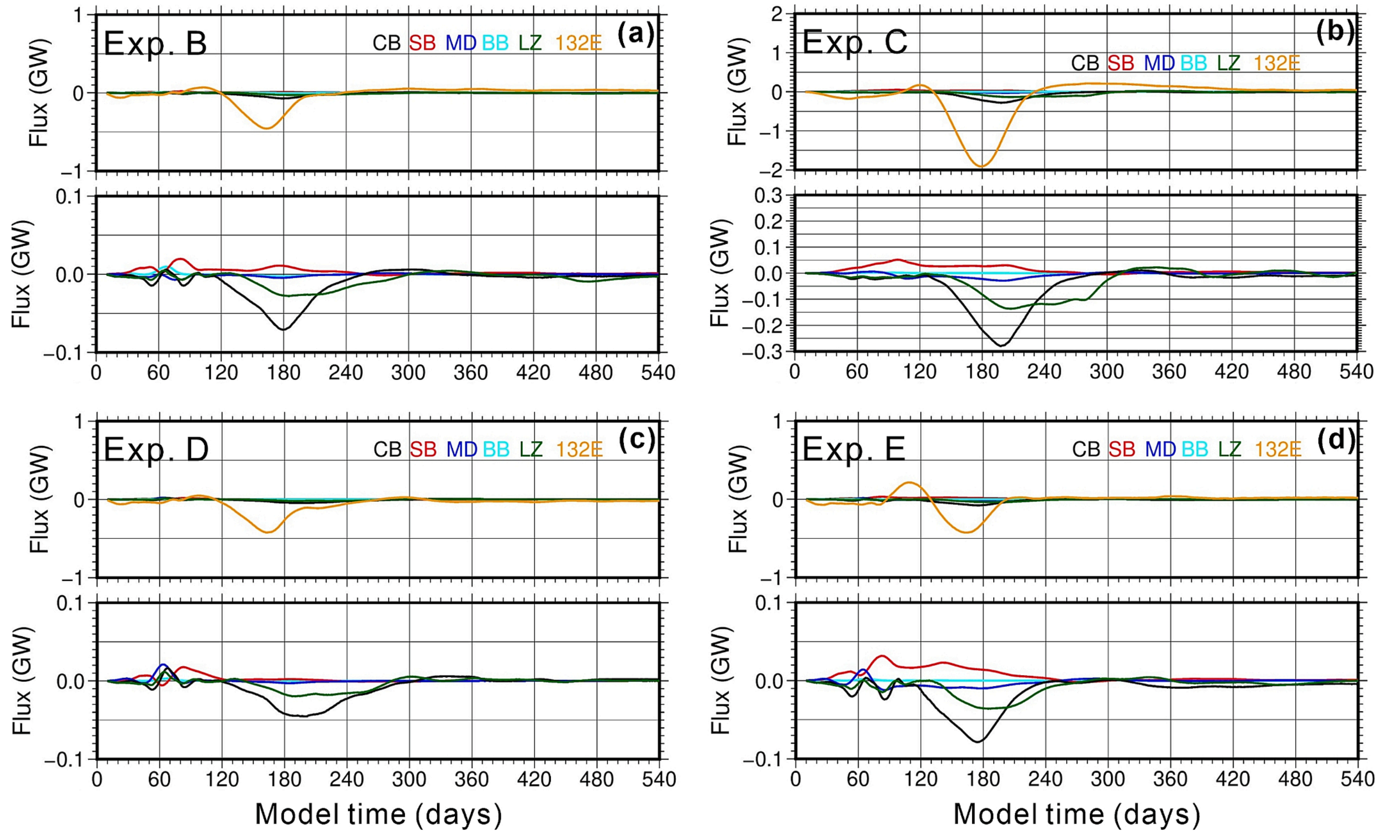

Fig. 11. Same as Fig. 9 but for Exps. (a) B, (b) C, (c) D, and (d) E.

time and space than those set and produced in our model. This difference suggests that it is challenging to clearly identify Rossby waves, particularly near the land-sea boundary, and to separate Rossby waves from reflected and forced Kelvin waves in satellite altimeter observations of SLAs as noted by Spall and Pedlosky (2005). For example, the longitudinal and temporal SLA variations along 10.5°N and 5°N suggest that the

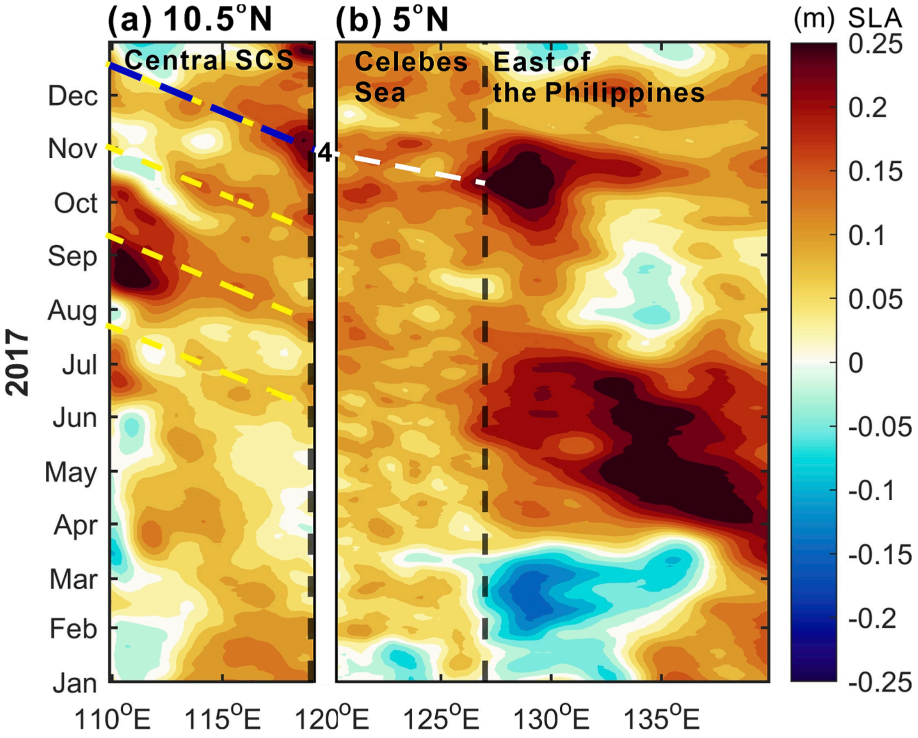

Fig. 12. Longitudinal and temporal variations in satellite SLA (a) between 110°E and 119°E along 10.5°N, similar to Fig. 1b, and (b) between 120°E and 140°E along 5°N. The "4″ indicates the fourth SLA oscillation event observed by Jan et al. (2021).

SLA crest off the eastern Philippines during 15 October and 15 November (Fig. 12b) may have contributed to the SLA oscillation off the west coast of Palawan (marked by "4" in Fig. 12a) during 25 October and 20 November. However, the SLA signal connecting the two SLA crests in the Celebes Sea is patchy and weak (Fig. 12b). The mean satellite SLA time series at the boxes selected in this study and the numerical results provide significant support for the dynamic connection of the two SLA crests.

Importantly, oceanic Rossby waves are crucial in influencing ENSO events, as they transverse the entire basin, and the coastal hydrography and ecology when the waves interact with the western boundary (Anderson and Gill, 1975; Anderson et al., 1979; Jacobs et al., 1993; Jacobs et al., 1994; Meyers et al., 1996; Chelton and Schlax, 1996; Jacobs et al., 1993; White et al., 1998; Uz et al., 2001; Cravatte et al., 2004; Stammer et al., 2008; Zhuang et al., 2013; Hu et al., 2022). The results of this study suggest that, in addition to atmospheric forcings, the transmission of tropical Rossby waves through the Philippines Archipelago might be a mechanism for transporting ENSO impacts into marginal seas such as the SCS and Indonesian seas, as suggested by Hu et al. (2022). Additionally, circulation, tidal dynamics, and seasonal hydrographic variations may influence the transmission of Rossby waves. Investigating these influences warrants careful consideration in future research.

5. Conclusions

The examination of satellite altimeter SLA data, combined with sea level measurements from fixed tide-gauge stations along the northern coast of the Sulu Sea, revealed the westward propagation of tropical Rossby waves within the western North Pacific Ocean. Potential intraseasonal Rossby waves, identified as either SLA crests or troughs, were traced from the central tropical Pacific to the western boundary along the east coast of the Philippines. The combined analysis of both satellite altimeter and tide-gauge SLA data indicated that these waves could propagate through the southern Philippine Archipelago and transmit into the central SCS. The estimated Rossby wave speed was approximately 0.68 m s^{-1}, which is comparable to the theoretical speed of Rossby waves at 5°N of 0.7 m s^{-1}; this value was ~0.67 m s^{-1} in the numerical simulations (Kessler, 1990).

By using a three-dimensional, primitive equation numerical model with 0.1° grid resolution in the western North Pacific, realistic topography, and idealized wind forcing for generating Rossby waves, we demonstrated the transmission of westward-propagating Rossby waves (or SLA signals) through the Philippine Archipelago. The model reproduced essential temporal and spatial variations analyzed from the SLA and coastal sea level data. As tropical SLA signals impinged on the Philippines' east coast at approximately 5°N–10°N, the westward energy flux bifurcated into a northward branch that entered the northern SCS along the east coast of Luzon and a southward branch that moved to the Celebes Sea. The southward branch was then transmitted through the Sibutu Passage into the Sulu Sea. The numerical results revealed that the energy flux hugged the western boundary of the Sulu Sea before it entered the central SCS through the Mindoro Strait.

Analysis of SLA energetics suggested that ~20 % and ~14 % of the westward-propagating energy passing through the 132°E section entered the Celebes Sea along the Philippines' southeastern coast and the northern SCS through the Luzon Strait, respectively. Among the energy that entered the Celebes Sea, ~16 % passed through the Sibutu Passage into the Sulu Sea, and ~12 % was transmitted through the Mindoro Strait into the central SCS. Approximately 34 % of the energy passing through the 132°E section entered the Celebes Sea and northern SCS, indicating that approximately 66 % of the incident energy was dissipated, transformed, scattered, or reflected at the western boundary. Ultimately, approximately 2–5 % of the incident SLA energy passing through the 132°E section could enter the central SCS via the Mindoro Strait. The transmission rate of incident SLA energy through the Mindoro Strait into the central SCS was sensitive to the latitude at which the Rossby wave impinged east of the Philippines. As the center of the incident SLA impinged at more southerly latitudes, the energy entering the central SCS increased significantly.

The northern Celebes Sea-Sibutu Passage-western Sulu Sea-Mindoro Strait pathway was crucial for transmitting SLA signals from east of the Philippines to the central SCS, connecting SLA and velocity variability in the central SCS and facilitating the generation of Rossby waves that emanated from the west coast of Palawan toward the western SCS, as observed by Jan et al. (2021) during the summer of 2017. This study confirmed that the aforementioned process was a physical mechanism contributing to the sea level and associated velocity oscillations in the central SCS. This perspective filled a critical gap in existing knowledge and highlighted the importance of the Philippine Archipelago as a key region for energy transmission in tropical ocean systems.

Declaration of Generative AI and AI-assisted technologies in the writing process

During the preparation of this work the authors used Grammarly.com–English Editing Software Service provided by the National Taiwan University. After using this tool/service, the authors reviewed and edited the content as needed and takes full responsibility for the content of the publication.

Data availability statement

Satellite SLA is obtained from CMEMS (accessible at https://doi.org/10.48670/moi-00148). Sea level records from tide-gauge stations in Palawan is available at https://doi.org/10.5281/zenodo.10396727. The numerical model code can be downloaded freely from the Mendeley Repository (Jan, S., 2025. Numerical model for studying Rossby wave transmission through the Philippine Archipelago, Mendeley Data, V1, doi: 10.17632/pr9f2jww8d.1).

CRediT authorship contribution statement

Mac Euan D. Malugao: Writing – review & editing, Writing – original draft, Visualization, Validation, Software, Investigation, Formal analysis, Data curation. **Sen Jan:** Writing – review & editing, Writing – original draft, Visualization, Validation, Supervision, Software, Methodology, Investigation, Funding acquisition, Formal analysis, Data curation, Conceptualization. **Ming-Huei Chang:** Writing – review & editing, Software, Methodology, Investigation, Data curation, Conceptualization. **Tung-Yuan Ho:** Writing – review & editing, Resources, Investigation, Funding acquisition. **Yiing Jang Yang:** Writing – review & editing, Investigation, Data curation.

Declaration of competing interest

The authors declare that they have no known competing financial interests or personal relationships that could have appeared to influence the work reported in this paper.

Acknowledgments

We sincerely thank the five anonymous reviewers for their insightful comments and suggestions, which greatly helped improved the content and clarity of the manuscript. NAMRIA Administrator Peter N. Tiangco provided the hourly coastal sea level data products. Yi-Chen Cheng helped plot Fig. 1a. This work was supported by the National Science and Technology Council (NSTC) of Taiwan. Taiwan International Graduate Program (TIGP) sponsors the scholarship of Mac Euan D. Malugao. SJ is sponsored under grants NSC-111-2611-M-002-020, NSC-111-2119-M-002-014, NSTC-112-2119-M-002-023, and NSTC-113-2119-M-002-034. MEDM is sponsored under grant NSTC-112-2119-M-002-023. TYH is sponsored by the NSTC.

Appendix A:. Configurations of the numerical model

Under the Bousinessq and hydrostatic approximation and using the σ–coordinate in the vrtical, transformed by $\sigma = (z-\eta)/(H+\eta)$, the governing equations of the Princeton Ocean Model comprise the momentum equation in the Cartesian coordinate x ,y, and z directions, continuity equation, and temperature and salinity equations, as follows (Blumberg & Mellor, 1987).

$$\frac{\partial UD}{\partial t}+ADV_U+\frac{\partial Uw}{\partial \sigma}-fVD=-GRAD_xP'+DIF_U+\frac{\partial}{\partial \sigma}\left(\frac{K_M}{D}\frac{\partial U}{\partial \sigma}\right) \tag{A1}$$

$$\frac{\partial VD}{\partial t}+ADV_V+\frac{\partial Vw}{\partial \sigma}+fUD=-GRAD_yP'+DIF_V+\frac{\partial}{\partial \sigma}\left(\frac{K_M}{D}\frac{\partial V}{\partial \sigma}\right) \tag{A2}$$

$$\frac{\partial P'}{\partial \sigma}=-\rho' \mathrm{gD} \tag{A3}$$

$$\frac{\partial \eta}{\partial t}+\frac{\partial UD}{\partial x}+\frac{\partial VD}{\partial y}+\frac{\partial w}{\partial \sigma}=0 \tag{A4}$$

$$\frac{\partial \varphi D}{\partial t}+ADV_\varphi+\frac{\partial w\varphi}{\partial \sigma}=DIF_\varphi+\frac{\partial}{\partial \sigma}\left(\frac{K_Z}{D}\frac{\partial \varphi}{\partial \sigma}\right) \tag{A5}$$

where (U, V) are horizontal velocity components in the x and y directions, w is the velocity component normal to σ-surface, D is total water depth (D=H + η), H is mean water depth and η is sea surface height relative to an equilibrium sea surface, t is time, f is the Coriolis parameter, ρ' is perturbation density, P' is perturbation pressure, (ADV_U, ADV_V), ($GRAD_xP'$, $GRAD_yP'$), and (DIF_U, DIF_V) are horizontal advection, pressure gradient and diffusion terms, respectively, in the horizontal momentum equations, g is the gravitational acceleration, φ represents temperature (T) or salinity (S), ADV_φ and DIF_φ are horizontal advection and diffusion terms, respectively, in temperature and salinity equations, and K_M and K_Z are vertical eddy viscosity and diffusivity, respectively. The horizontal eddy viscosity and diffusivity are determined using the Smagorinsky formulation (Smagorinsky, 1963), and the vertical viscosity and diffusivity are determined by the level-2.5 turbulence closure scheme of Mellor and Yamada (1982). Bottom stress is calculated by a quadratic stress law, $C_z\left(U^2+V^2\right)^{\frac{1}{2}}(U,V)$, where the non-dimensional drag coefficient C_z is derived to produce a logarithmic bottom boundary layer based on a specified bottom roughness length of 0.01 m.

There are 41 uneven σ–layers in the vertical σ–coordinate. The normalized center of each vertical grid between 0 and –1 in the σ–coordinate is –0.001, –0.003, –0.005, –0.007, –0.009, –0.011, –0.013, –0.015, –0.017, –0.020, –0.023, –0.027, –0.031, –0.035, –0.039, –0.043, –0.047, –0.051, –0.056, –0.060, –0.064, –0.068, –0.072, –0.076, –0.080, –0.084, –0.088, –0.093, –0.100, –0.126, –0.146, –0.177, –0.218, –0.259, –0.331, –0.434, –0.537, –0.691, and –0.897 from the top to the bottom layer, respectively.

The initial temperature profile at each grid is computed using the formula

$$T(z)=2+25e^{\left(\frac{z}{1000}\right)} \tag{A1}$$

where z is depth in meters. The corresponding density profile is derived from this temperature profile, assuming a constant salinity of 34.5. The heat flux at the sea surface is set to zero. An idealized wind forcing is applied at the sea surface to only generate sea level variations in association with Rossby waves. The wind stress is given as

$$\tau=\tau_{max}e^{-\left[\frac{x-x_0}{L_x}\right]^2-\left[\frac{y-y_0}{L_y}\right]^2}\sin\left(\frac{\pi t}{T_w}\right) \tag{A2}$$

where τ_{max} is a prescribed wind stress amplitude, x and y are longitude and latitude, respectively, (x_0, y_0) is the center location of wind field in longitude and latitude, respectively, L_x and L_y are the half Gaussian distribution (in degrees) of wind field in the zonal and meridional directions, respectively, and T_w is duration of wind stress applied to the model. In a baseline model run, an easterly wind field centered at (6°N, 160°W) is set, with $\tau_{max} = 0.2$ N m^{-2}, L_x and L_y as 5 and 4 degrees in the zonal and meridional directions, respectively, and $T_w = 30$ d from the beginning of the numerical integration. The wind stress field is shown in Fig. A1. The total integration time for a numerical experiment is 540 days, with time steps of 15 s for the external mode and 600 s for the internal mode. Daily data on velocity, sea level, and hydrography are stored in a separate file for further analysis.

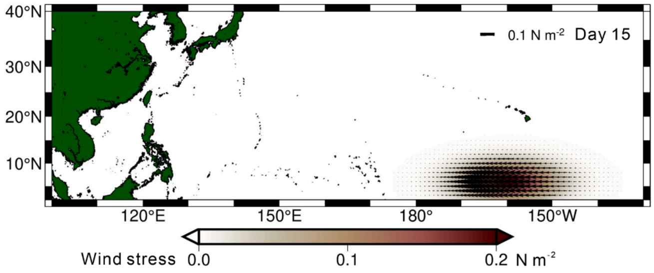

Fig. A1. Maximum wind stress (color shading and arrows) applied in the model.

Appendix B. Supplementary data

Supplementary data to this article can be found online at https://doi.org/10.1016/j.pocean.2025.103481.

Data availability

The numerical model code can be downloaded freely from the Mendeley Repository (https://… will be provided upon the acceptance of this manuscript)

References

Anderson, D.L.T., Gill, A.E., 1975. Spin-up of a stratified ocean, with applications to upwelling. Deep Sea Res. and Oceanogr. Abstracts 22 (9), 583–596. https://doi.org/10.1016/0011-7471(75)90046-7.

Anderson, D.L.T., Bryan, K., Gill, A.E., Pacanowski, R.C., 1979. The transient response of the North Atlantic: Some model studies. J. Geophys. Res., 84 (C8), 4795. https://doi.org/10.1029/JC084iC08p04795.

Apel, J.R., Holbrook, J.R., Liu, A.K., Tsai, J.J., 1985. The Sulu Sea internal soliton experiment. J. Phys. Oceanogr., 15, 1625–1651.

Battisti, D.S., 1989. On the role of off-equatorial oceanic Rossby waves during ENSO. J. Phys. Oceanogr., 19, 551–560. https://doi.org/10.1175/1520-0485(1989)019<0551:OTROOE>2.0.CO;2.

Blumberg, A.F., Mellor, G.L., 1987. A description of a three-dimensional coastal ocean circulation model. In: Heaps, N.S. (Ed.), Coastal and Estuarine Sciences, Book 4. American Geophysical Union, Washington D.C., pp. 1–6

Cabanes, C., Huck, T., Colin de Verdière, A., 2006. Contributions of wind forcing and surface heating to interannual sea level variations in the Atlantic Ocean. J. Phys. Oceanogr., 36 (9), 1739–1750. https://doi.org/10.1175/JPO2935.1.

Cabrera, O.C., Villanoy, C.L., David, L.T., Gordon, A.L., 2011. Barrier layer control of entrainment and upwelling in the Bohol Sea. Philippines. Oceanogr., 24 (1), 130–141. https://doi.org/10.5670/oceanog.2011.10.

Cai, M., Huang, B., 2013. A dissection of energetics of the geostrophic flow: Reconciliation of Rossby wave energy flux and group velocity. J. Atmos. Sci., 70, 2179–2196. https://doi.org/10.1175/JAS-D-12-0249.1.3.

Calafat, F.M., Wahl, T., Lindsten, F., Williams, J., Frajka-Williams, E., 2018. Coherent modulation of the sea-level annual cycle in the United States by Atlantic Rossby waves. Nat. Commun., 9 (1). https://doi.org/10.1038/s41467-018-04898-y.

Cessi, P., Primeau, F., 2001. Dissipative selection of low-frequency modes in a reduced-gravity basin. J. Phys. Oceanogr., 31, 127–137. https://doi.org/10.1175/1520-0485(2001)031<0127:DSOLFM>2.0.CO;2.

Chelton, D.B., Schlax, M.G., 1996. Global observations of oceanic Rossby waves. Sci., 272 (5259), 234–238. https://doi.org/10.1126/science.272.5259.234.

Chelton, D.B., DeSzoeke, R.A., Schlax, M.G., El Naggar, K., Siwertz, N., 1998. Geographical variability of the first baroclinic Rossby radius of deformation. J. Phys. Oceanogr., 28, 433–460. https://doi.org/10.1175/1520-0485(1998)028<0433:GVOTFB>2.0.CO;2.

Chern, C.-S., Jan, S., Wang, J., 2010. Numerical study of mean flow patterns in the South China Sea and the Luzon Strait. Ocean Dyn., 60 (5), 1047–1059. https://doi.org/10.1007/s10236-010-0305-3.

Clarke, A.J., 1991. On the reflection and transmission of low-frequency energy at the irregular Pacific Ocean boundary. J. Geophys. Res., 96, 3289–3305. https://doi.org/10.1029/90JC00985.

Cravatte, S., Boulanger, J.-P., Picaut, J., 2004. Reflection of intraseasonal equatorial Rossby waves at the western boundary of the Pacific Ocean, Geophys. Res. Lett., 31, L10301. https://doi.org/10.1029/2004GL019679.

du Penhoat, Y., Cane, M.A., 1991. Effect of low-latitude western boundary gaps on the reflection of equatorial motions. J. Geophys. Res., 96 (S1), 3307–3322. https://doi.org/10.1029/90JC01798.

Durland, T.S., Farrar, J.T., 2020. Another note on Rossby wave energy flux. J. Phys. Oceanogr., 50, 531–534. https://doi.org/10.1175/JPO-D-19-0237.1.

Giese, B.J., Harrison, D.E., 1990. Aspects of the Kelvin wave response to episodic wind forcing. J. Geophys. Res., 95, 7289–7312. https://doi.org/10.1029/JC095iC05p07289.

Gordon, A.L., Huber, B.A., Metzger, E.J., Susanto, R.D., Hurlburt, H.E., Adi, T.R., 2012. South China Sea throughflow impact on the Indonesian throughflow. Geophys. Res. Lett., 39, L11602. https://doi.org/10.1029/2012GL052021.

Hu, X., Xue, H., Liang, L., 2022. Impact of ENSO on the entrance of the Indonesian Throughflow: The oceanic wave propagation. J. Geophys. Res.: Oceans 127, e2022JC018782. https://doi.org/10.1029/2022JC018782.

Jacobs, G.A., Emery, W.J., Born, G.H., 1993. Rossby waves in the Pacific Ocean extracted from Geosat altimeter data. J. Phys. Oceanogr., 23 (6), 1155–1175. https://doi.org/10.1175/1520-0485(1993)023<1155:RWITPO>2.0.CO;2.

Jacobs, G.A., Hurlburt, H.E., Kindle, J.C., Metzger, E.J., Mitchell, J.L., Teague, W.J., Wallcraft, A.J., 1994. Decade-scale trans-Pacific propagation and warming effects of an El Niño anomaly. Nature 370 (6488), 360–363. https://doi.org/10.1038/370360a0.

Jan, S., Chern, C.-S., Wang, J., Chao, S.-Y., 2007. Generation of diurnal K_1 internal tide in the Luzon Strait and its influence on surface tide in the South China Sea. J. Geophys. Res. Oceans C06019. https://doi.org/10.1029/2006JC004003.

Jan, S., Lien, R.-C., Ting, C.-H., 2008. Numerical study of baroclinic tides in Luzon Strait. J. Oceanogr., 64 (5), 789–802. https://doi.org/10.1007/s10872-008-0066-5.

Jan, S., Mensah, V., Andres, M., Chang, M.-H., Yang, Y.J., 2017. Eddy-Kuroshio interactions: Local and remote effects. J. Geophys. Res. Oceans 122, 9744–9764. https://doi.org/10.1002/2017JC013476.

Jan, S., Chang, M.H., Yang, Y.J., Sui, C.H., Cheng, Y.H., Yeh, Y.Y., Lee, C.W., 2021. Mooring observed intraseasonal oscillations in the central South China Sea during summer monsoon season. Sci. Rep., 11 (1). https://doi.org/10.1038/s41598-021-93219-3.

Kessler, W.S., 1990. Observations of long Rossby waves in the northern tropical Pacific. J. Geophys. Res., 95 (C4), 5183–5217. https://doi.org/10.1029/JC095iC04p05183.

Li, M., Wei, J., Wang, D., Gordon, A.L., Yang, S., Malanotte-Rizzoli, P., Jiang, G., 2019. exploring the importance of the Mindoro-Sibutu Pathway to the upper-layer circulation of the South China Sea and the Indonesian Throughflow. J. Geophys. Res. Oceans 124, 5054–5066. https://doi.org/10.1029/2018JC014910.

Li, M., Xue, H., Wei, J., Liang, L., Gordon, A.L., Yang, S., 2021. The role of the Mindoro-Sibutu pathway on the South China Sea multi-layer circulation. J. Phys. Oceanogr., 51, 2767–2782. https://doi.org/10.1175/JPO-D-20-0165.1.

Mellor, G.L., Yamada, T., 1982. Development of turbulence closure model for geophysical fluid problems. Rev. Geophys., 20, 851–875. https://doi.org/10.1029/RG020i004p00851.

Mensah, V., Ohshima, K.I., 2020. Variabilities of the sea surface height in the Kuril Basin of the Sea of Okhotsk: coherent shelf-trapped mode and Rossby normal modes. J. Phys. Oceanogr., 50, 2289–2313. https://doi.org/10.1175/JPO-D-19-0216.1.

Metzger, E. J., Hurlburt, H. E., 1996. Coupled dynamics of the South China Sea, the Sulu Sea, and the Pacific Ocean. J. Geophys. Res., 101, 12 331–12 352, Doi: 10.1029/95JC03861.

Meyers, S.D., Liu, M., O'Brien, J.J., Johnson, M.A., Spiesberger, J.L., 1996. Interdecadal variability in a numerical model of the Northeast Pacific Ocean: 1970–89. J. Phys. Oceanogr., 26 (12), 2635–2652. https://doi.org/10.1175/1520-0485(1996)026<2635:IVIANM>2.0.CO;2.

Pawlowicz, R., Beardsley, B., Lentz, S., 2002. Classical tidal harmonic analysis including error estimates in MATLAB using T_TIDE. Comput. Geosci., 28 (8), 929–937. https://doi.org/10.1016/S0098-3004(02)00013-4.

Pujol, M.I., Faugère, Y., Taburet, G., Dupuy, S., Pelloquin, C., Ablain, M., Picot, N., 2016. DUACS DT2014: The new multi-mission altimeter data set reprocessed over 20 years. Ocean Sci., 12 (5), 1067–1090. https://doi.org/10.5194/os-12-1067-2016.

Qiu, B., Chen, S., 2004. Seasonal modulations in the eddy field of the South Pacific Ocean. J. Phys. Oceanogr., 34 (6), 1515–1527. https://doi.org/10.1175/1520-0485(2004)034<1515:SMITEF>2.0.CO;2.

Qiu, B., 2003. Kuroshio Extension variability and forcing of the Pacific Decadal Oscillations: Responses and potential feedback. J. Phys. Oceanogr., 33 (12), 2465–2482. https://doi.org/10.1175/2459.1.

Robert, C.P., Casella, G., 2004. Monte Carlo Statistical Methods, 2nd ed.

Smagorinsky, J.S., 1963. General circulation experiments with the primitive equations: I. The Basic Experiment. Mon. Weather Rev., 91, 99–164. https://doi.org/10.1175/1520-0493(1963)091<0099:GCEWTP>2.3.CO;2.

Spall, M.A., Pedlosky, J., 2005. Reflection and transmission of equatorial Rossby Waves. J. Phys. Oceanogr., 35 (3), 363–373. https://doi.org/10.1175/JPO-2691.1.

Stammer, D., Park, S., Köhl, A., Lukas, R., Santiago-Mandujano, F., 2008. Causes for large-scale hydrographic changes at the Hawaii Ocean time series station. J. Phys. Oceanogr., 38 (9), 1931–1948. https://doi.org/10.1175/2008JPO3751.1.

Tessler, Z.D., Gordon, A.L., Jackson, C.R., 2012. Early stage soliton observations in the Sulu Sea. J. Phys. Oceanogr., 42, 1327–1336. https://doi.org/10.1175/JPO-D-11-0165.1.

Uz, B.M., Yoder, J.A., Osychny, V., 2001. Pumping of nutrients to ocean surface waters by the action of propagating planetary waves. Nature 409 (6820), 597–600. https://doi.org/10.1038/35054527.

Villanoy, C.L., Cabrera, O.C., Yñiguez, A., Camoying, M., de Guzman, A., David, L.T., Lament, P.F., 2011. Monsoon-driven coastal upwelling off Zamboanga peninsula. Philippines. Oceanogr., 24 (1), 156–165. https://doi.org/10.5670/oceanog.2011.12.

Webber, B.G.M., Matthews, A.J., Heywood, K.J., Stevens, D.P., 2011. Ocean Rossby waves as a triggering mechanism for primary Madden–Julian events. Q. J. R. Meteorol. Soc., 138 (663), 514–527. https://doi.org/10.1002/qj.936.

Wei, J., Li, M.T., Malanotte-Rizzoli, P., Gordon, A.L., Wang, D.X., 2016. Opposite variability of Indonesian Throughflow and South China Sea Throughflow in the Sulawesi Sea. J. Phys. Oceanogr., 46, 3165–3180. https://doi.org/10.1175/JPO-D-16-0132.1.

White, W.B., Chao, Y., Tai, C.-K., 1998. Coupling of biennial oceanic Rossby waves with the overlying atmosphere in the Pacific basin. J. Phys. Oceanogr., 28 (6), 1236–1251. https://doi.org/10.1175/1520-0485(1998)028<1236:COBORW>2.0.CO;2.

Xie, S.-P., Chang, C.-H., Xie, Q., Wang, D., 2007. Intraseasonal variability in the summer South China Sea: Wind jet,cold filament, and recirculations. J. Geophys. Res., 112, C10008. https://doi.org/10.1029/2007JC004238.

Zang, X., Fu, L.L., Wunsch, C., 2002. Observed reflectivity of the western boundary of the equatorial Pacific Ocean. J. Geophys. Res., 107 (10). https://doi.org/10.1029/2000jc000719.

Zhuang, W., Qiu, B., Du, Y., 2013. Low-frequency western Pacific Ocean sea level and circulation changes due to the connectivity of the Philippine Archipelago. J. Geophys. Res. Oceans 118, 6759–6773. https://doi.org/10.1002/2013JC009376.